scientific reports

Check for updates

OPEN

Microbial responses under sunlight-dark conditions accelerate sequestration and transformation of soil biogenic, redox and non-redox components, including As and Hg

Mohammad Mohinuzzaman[1,8], Jie Zhang[1,2], M. G. Khan Mostofa[1,2]✉, Ruoyu Sun[1,3], Wang Zheng[1,3], Jiubin Chen[1,2], Nicola Senesi[3], Giorgio S. Senesi[4], Davide Vione[5,6], Si-Liang Li[1,2], Jie Yuan[7] & Cong-Qiang Liu[1,2]✉

Climatic warming and the resulting increase in soil respiration affect the sequestration and transformation of soil components, as well as their transport to the surrounding ecosystems. However, the integrated mechanistic details of these processes remain elusive. Here we apply an extraction protocol that utilizes two sequential extraction techniques to isolate and analyze both dissolved and solid-state soil components and to assess their dark and photoinduced fates under varying temperature conditions, intended to simulate global warming. We observe a net increase in total sulfur (1.2–41.0%), which is ascribed to S sequestration-redox reactions involving both sulfide oxidation to $S^0 \rightleftharpoons SO_4^{2-}$ and the reverse ($S^{2-}/S_2^{2-} \rightleftharpoons SO_4^{2-}$) via SO_4^{2-} plus soil organic sulfur plus sulfides/pyrites (SOS + S_n^{2-}) decrease and/or increase under sunlight, dark, and control conditions. Higher transformation and mineralization of various components occurs in dark/microbial conditions by the wide day-night experimental temperature variation (10–42 °C) in comparison with the control at constant temperature (25 °C). Remarkably, the photosynthetically-derived soil organic carbon (SOC)/humic substances (HS)-bound mineral neoformation through uptake and sequestration of various components, including As and Hg, is specifically detected under sunlight and control conditions. A major role is played by seven redox-active metals (Fe, Mn, Cu, Hg, Ni, As, and U), which are involved in both organo-mineral complexation and redox processes. Importantly, the dark/microbial dissolution of iron minerals is primarily responsible for the increased export of water-extractable or labile As (33.8–89.7%) over a period of 0-150 days, with no evidence of sequestration. In contrast, As sequestration and relatively low water-extractable As export occur under sunlight (9.0-25.5%) and control (17.4–38.4%) samples. A net decrease in Hg levels is observed over a period of 0 to 150 days, along with relatively low sequestration across three treatments, appearing the highest losses under sunlight conditions (9.8–17.4%) when compared to dark (5.2–11.4%) and control (3.6–11.6%) samples. This effect may be attributed to the reduction of Hg(I, II)–DOM into gaseous Hg^0. These findings could assist in managing soil components and predicting where and when the side effects of global warming-such as erosion-associated mobilization of soil components, including As and Hg into surrounding surface water, groundwater, and the atmosphere-are likely to manifest.

Keywords Luvisol/forest soil, Sunlight/Dark/control, Soil components, Including C, S, N, P, Si and metals, Sequestration, Transformation

Abbreviations

LS	Labile state
CS	Complexed state
COS	Carbonyl sulfide
Hg_T	Total mercury
DIC_{LS+CS}	Dissolved inorganic carbon in LS and CS
DOC_{LS+CS}	Dissolved organic carbon in LS and CS
δ^{13}C-DOC	Stable carbon isotopes in DOC
DOM	Dissolved organic matter
DON_{LS+CS}	Dissolved organic nitrogen in LS and CS
HS	Humic substances
SIC	Soil inorganic carbon
SOC	Soil organic carbon
δ^{13}C-SOC	Stable carbon isotopes in SOC
$SOS+S_n^{2-}$	Soil organic sulfur plus sulfides/pyrites (S_n^{2-})
STC	Soil total carbon
δ^{13}C-STC	Stable carbon isotopes in STC
STN	Soil total nitrogen
STS	Soil total sulfur
δ^{15}N-STN	Stable nitrogen isotopes in STN
$M_{LS+CS\ or\ LS\ or\ CS}$	Metals measured in LS and/or CS (M = Fe, Mn, Cu, Hg, Ni, As, U, Al, Ca, Mg or Sr)

[1]School of Earth System Science, Tianjin University, 92 Weijin Road, Tianjin 300072, China. [2]Tianjin Key Laboratory of Earth Critical Zone Science and Sustainable Development in Bohai Rim, Tianjin University, 92 Weijin Road, Tianjin 300072, China. [3]Diparment to di Scienze del Suolo, Università degli Studi di Bari "Aldo Moro", della Pianta e degli Alimenti, Via G. Amendola 165/A, Bari 70126, Italy. [4]CNR - Istituto per la Scienza e Tecnologia dei Plasmi (ISTP) - sede di Bari, Via Amendola, 122, Bari D - 70126, Italy. [5]Dipartimento di Chimica, Università degli Studi di Torino, Via P. Giuria 5, Torino 10125, Italy. [6]Centro Interdipartimentale NatRisk, Via Leonardo da Vinci 44, Grugliasco (TO) 10095, Italy. [7]College of Resources and Environment, Xingtai University, Quanbei East Road 88, Qiaodong District, Xingtai, Hebei, China. [8]Present address: Department of Environmental Science and Disaster Management, Noakhali Science and Technology University, Noakhali, Bangladesh. ✉email: mostofa@tju.edu.cn; liucongqiang@tju.edu.cn

The majority of the Earth's terrestrial carbon is stored in the soil, the top of which is primarily exposed to sunlight[1–4] and intense microbial activity[5,6]. Climate scenarios forecast the loss of 55 ± 50 Pg of C from upper soil horizons by 2050, and each °C increase in temperature would reduce the total soil organic carbon (SOC) stocked by 30 ± 30 to 203 ± 161 Pg of C[5]. Furthermore, the worldwide increasing land use and land cover changes, e.g., by deforestation and drought[7,8] favor SOC losses by enhanced soil respiration[6,9], erosion[8], and temperature-induced degradation[7,10]. These effects are expected to reduce soil C storage[11,12] and C sequestration/stability[13,14], thereby affecting land degradation[15,16]. Generally, biodegradation processes are mainly responsible for SOC losses with emissions of CO_2, COS, and H_2S[10,17,18], whereas sunlight-exposed SOC may produce CO_2[19] and NO_x emissions[1,3]. These phenomena involve various soil biogeochemical processes, including SOC transformations[20,21], soil oxygenic/anoxygenic photosynthesis[22,23], soil respiration accelerated by temperature increase[6,9], dissolution of redox and non-redox metals from minerals[4,13,14,24–27], and As release[28,29]. Specifically, transformation and mineralization processes occur for SOC and humic substances (HS) associated with clay, and Fe-like minerals[13,24,25,30] at the mineral-microbes interfaces, *via* reactive oxygen species generated from mineral-induced electron transfer[14], Fe-mediated processes in humid soils[25], and/or reductive dissolution of clay minerals[14,31]. These processes highlight the absence of unique potential mechanisms of SOC mineralization. Based on this research gap, the key scientific question emerges: is SOM involved in the integrated mechanism of mineralization of HS-associated organo-minerals and their subsequent sequestration or neoformation, along with the export of various dissolved and gaseous components into surface water, groundwater, and/or the atmosphere?

Moreover, mineral sequestration of SOC[22,23] may occur via subsequent sequestration/uptake of carbon (C)[32–35], sulfur (S)[36,37], nitrogen (N)[1,38,39], and various metals, including Hg[4,24,25,30,40–42], which are mostly responsible for the neoformation of organo-mineral components[24,25,30,32,43,44] that are involved in SOC stabilization and accumulation[13,45]. Such transformations and sequestration of soil organo-mineral components occur simultaneously in the soil matrix, but any proved experimental evidence of the various responsible processes and factors that drive these phenomena, as well as their mechanisms, remain mostly uncertain. Based on this research gap, another key scientific question emerges: do raw soils under sunlight and microbial/dark treatments experience field conditions that help us understand the sequestration of C, S, N, and various metals, as well as the subsequent transformation processes of soil organic matter (SOM)?

Many researchers have employed various techniques to extract soil HS as individual fractions, i.e., humic acids (HA), fulvic acids (FA) and protein-like substances (PLS), as well as to assess the solubility of soil HS components using different extraction times ranging from 10 min to 24 h. For extracting HA and FA, the extraction methods used include the IHSS method, which involves 0.1 M HCl extraction followed by 0.1 M NaOH extraction[46], a modified IHSS method[47,48], or $Na_4P_2O_7$ mixed NaOH extraction[49], and the Nagoya University method, which involves alkaline extraction using Na_2SO_4 mixed with 0.1 M NaOH[50,51]. The solubility characteristic methods includes various extraction solutions such as pure water[52–54], alkaline solutions[54,55], acid solutions using 2.5 M and 13 M H_2SO_4 at 105°C[56], saline solutions[57], hot water (up to 100 °C) extraction[58–60],

various solid to liquid ratios[61], sequential extraction[62], and pH variation[61]. Among these extraction methods, water extracts at room temperature (or 25 °C) represent the labile components of SOM, while alkaline extracts represent the organo-mineral components of SOM influenced by environmental conditions and factors in soils and sands[20,54,63]. All other methods have been considered irrelevant to the environmental conditions and factors of the soil[20,54,63]. In particular, the use of individual water and alkaline soil extracts with inconsistent timescales remains a research gap, highlighting the need to develop a systematic, time-dependent extraction method that is highly efficient not only yielding soil components but also in reducing extraction time[54]. Moreover, solely relying on solid-phase analysis[13,14,64–66] does not accurately represent or estimate the exact contributions of soil labile and organo-mineral fractions. Additionally, this approach fails to account for the continuous leaching or export of soil components through water and/or rainwater runoff from terrestrial soils into surrounding surface water and groundwater ecosystems. Based on this research gap, another key scientific question emerges: how can soils (treated and untreated) be analyzed to gain a better understanding of their relevant components that remain in labile (water-extractable) and organo-mineral (alkaline extracts) forms, while also maximizing the efficiency of soil extracts with a shorter extraction time[21]?

Within the framework of these research gaps on studying SOM dynamics under existing ambient conditions[14,20,54], we propose three hypotheses. First, the photosynthetic uptake/sequestration of C, N, S, and various metals from soils or the atmosphere drives the growth and survival of soil microorganisms, which in turn leads to the generation of extracellular polymeric substances (EPS) and sulfur-mediated sequestration-redox processes ($S^{2-} \rightleftharpoons S^{o}$ and $S^{o} \rightleftharpoons SO_4^{2-} \rightleftharpoons S^{2-}/S_2^{2-} \rightleftharpoons SO_4^{2-}$). Second, the degradation of soil components, including EPS, driven by photosynthetically mediated S sequestration-redox processes, is coherently involved in organo-mineral neoformation, which persists in soils to maintain steady-state SOC levels, as well as the continuous export, leaching, or emission of degradative labile soil components from terrestrial soils into surrounding environments. Third, specific time-dependent water extraction (targeting labile components), followed by alkaline extraction (targeting organo-mineral components), for any soil can respectively represent the biogeochemical lability and organo-mineral stability of soil components under various soil conditions and factors.

To implement these three hypotheses, the main objectives of this work are to: *(i)* develop a comprehensive methodological procedure to separately extract soil labile and organo-mineral components; *(ii)* analyze the contents of C, S, N, P, and their respective nutrient or ending derivatives, as well as seven redox (Fe, Mn, Cu, Hg, Ni, As, and U) and four non-redox metals (Al, Ca, Mg, and Sr), soil total nitrogen (STN), soil total sulfur (STS), SOC, and soil inorganic carbon (SIC), as well as their stable isotopes in both the original soil and the soil residue after extraction, after 150 consecutive days of exposure to selected sunlight, dark, and control conditions, in order to achieve a robust understanding of the integrated transformation-sequestration of soil mineral components; and *(iii)* investigate the continuous export of dissolved-phase components potentially important for ecosystem functions and processes and also their subsequent sequestration for SOC stabilization, analyze the soil samples for their dissolved organic carbon (DOC), dissolved inorganic carbon (DIC), SO_4^{2-}, N-nutrients, P-nutrients, and dissolved SiO_3^{2-} contents, plus the fluorescence properties of HS in both water extracts (labile state, LS) and alkali-extracts (complexed state, CS). To achieve the objectives outlined above, various experiments are carried out in both field and laboratory settings in a wide temperature range (10–42 °C and 25 °C, respectively) to assess the potential effects that would be induced by global warming.

Results

Carbon transformation

Soil total carbon (STC) fluctuates, either increasing or decreasing under sunlight, dark, and control samples over various timescales, showing the highest increase in sunlight (by 0.43%) and the lowest decrease in dark conditions (by 10.8%; Fig. 1A). This increase in STC primarily results from a rise in soil inorganic carbon (SIC) in the sunlight and control treatments (Fig. S1A), suggesting that inorganic carbon sequestration occurs through photosynthetic uptake of CO_2 or DIC[17,33–35]. Moreover, the SOC decrease follows the order: dark > control > sunlight (Fig. 1B), which correspondingly reflects the DOC_{LS+CS} mineralization in the same order under dark and control conditions (Fig. 1C, D). In particular, the highest level of mineral-associated DOC_{CS} mineralization observed during the incubation period (by 10.0-35.2%), combined with a relatively low decrease in DOC_{LS} (by 9.3–15.5%), results in the highest level of SOC (by 6.4–10.8%) mineralization in the dark samples (Fig. 1C, D). This finding suggests the occurrence of microbial SOC transformation[20,21] *via* heterotrophic soil respiration[6,9,10,25]. Such changes would produce DIC_{LS+CS} or CO_2, COS or H_2S[11,17,18], and/or carbonate minerals by silicate weathering[67]. These phenomena can be induced in the dark by various microbial communities that are highly active in the day-night experimental temperature range (10–42 °C)[66,68]. Similarly, SOC or DOC transformation further supports the extended and/or partial mineralization of labile and complexed state forms of protein-like substances or fulvic acids, and the labile form of humic acids, as shown by fluorescence data[21] (Figs. S2-S3). The occurrence of carbonate mineral sequestration[67] is supported by the individual SIC increase and significant DIC_{LS+CS} decrease, together with stable isotope of STC (δ^{13}C-STC) enrichment (Fig. 1F and Fig. S1A-C). Remarkably, the gradual depletion of δ^{13}C-SOC and the fluctuations of δ^{13}C-DOC in both labile or complexed state forms in the dark (Fig. 1E, G,H) suggest that microbial SOC sequestration would occur via lighter DIC_{LS+CS}/CO_2 uptake, after inorganic carbon production from SOC + DOC_{LS+CS} mineralization[17,34,35]. This phenomenon often goes undetected when monitoring the SOC alone, because of the overwhelming role of mineralization. Similarly, in the control at constant temperature, a moderate level of SOC mineralization and/or respiration (2.3-6.0%) would account for relatively low microbial respiration by temperature-dependent specific microbial activities at the experimental temperature (25 °C)[6,66,68]. This phenomenon results in relatively low mineral-associated DOC_{CS} mineralization by 15.0% over the 0-30-75-150 day periods, while simultaneously causing a significant decrease by 28.7% in labile DOC_{LS} over the 0-30-75 day periods, which is reversed under

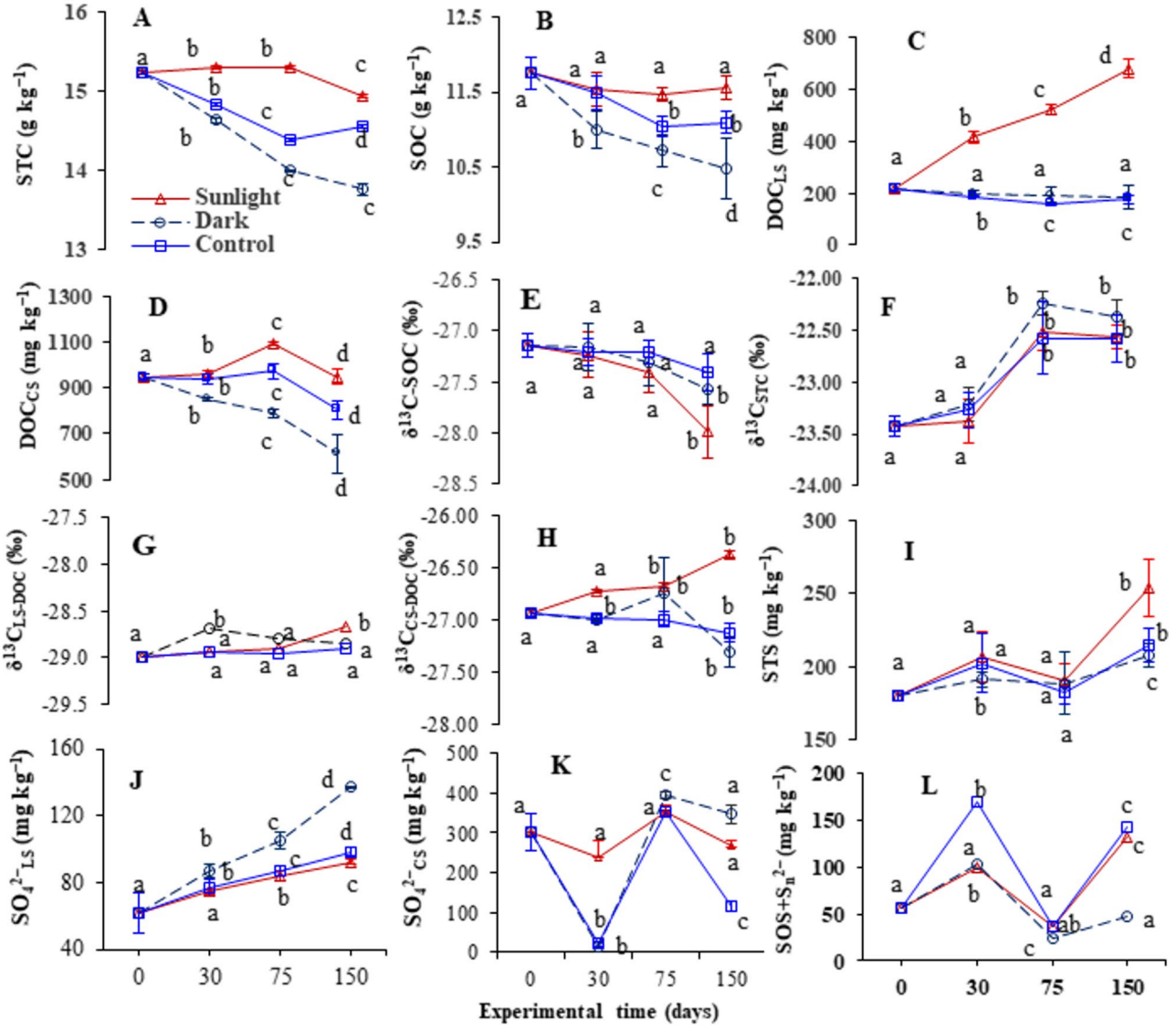

Fig. 1. Photoinduced and microbial changes of: soil total carbon (STC, **A**), soil organic carbon (SOC, **B**), dissolved organic carbon (DOC) concentration in labile state (DOC_{LS}, **C**) and complexed state (DOC_{CS}, D), stable isotope of soil organic carbon ($\delta^{13}C_{SOC}$, **E**), stable isotope of soil total carbon ($\delta^{13}C_{STC}$, **F**), δ^{13}C-DOC_{LS} (**G**), δ^{13}C-DOC_{CS} (**H**), soil total sulfur (STS, **I**), $SO_4^{2-}{}_{LS}$ (J), $SO_4^{2-}{}_{CS}$ (**K**) and soil organic sulfur (SOS) + sulfides/pyrites (S_n^{2} (**L**) in extracts from soils subjected to sunlight, dark and control conditions measured at time 0 (original soil) and after 30, 75 and 150 consecutive experimental days. Error bars indicate the standard deviation among three replicates. The average values labeled with different letters (a, b, ab, c, d) at various time period (0, 30, 75, and 150 days) indicate significant differences ($p < 0.05$) among the three treated samples (sunlight, dark, and control at constant temperature), as determined by a one-way ANOVA.

dark conditions. Furthermore, the observed depletion of δ^{13}C-SOC from −27.15‰ to −27.41‰ during the incubation period in the control samples (Fig. 1E) suggests that some degree of SOC sequestration, approximately a 0.4% increase, would occur in parallel (Fig. 1B). This happens because biologically generated SOC is coherently enriched in ^{12}C, due to the lighter DIC and/or CO_2 uptake caused by the SOC + DOC_{LS+CS} mineralization. The highest degree of δ^{13}C depletion (Figs. 1E) occurs under sunlight by photosynthetic uptake of lighter DIC or CO_2. Such changes are further highlighted by the high δ^{13}C-STC enrichment over 0–75 days, which remains primarily stable afterwards (Fig. 1F). Ideally, δ^{13}C-STC enrichment would arise primarily from the combined effects of lighter SOC + DOC_{LS+CS} mineralization and carbonate sequestration, with SIC increasing over individual timescale under all conditions (Fig. 1FSA). This finding agrees with the enrichment of δ^{13}C-SIC and δ^{13}C-SOC in soil depth-profiles elsewhere[33]. For instance, C respiration and sequestration processes can be induced by bacterial and fungal communities[6,11,66,68] during both oxygenic and anoxygenic photosynthesis either through lichen-associated soil fungi plus cyanobacterial symbioses[22,23,38,69] and/or non-symbiotic pathways[70–72]. Soil photosynthetic processes are further supported by the results from 100 soil samples collected across China, which demonstrated that lighter or depleted δ^{13}C-SOC values (-27.4‰ to -22.5‰) correlated with higher levels

of soil components, including Hg species, while enriched δ^{13}C-SOC (-22.5‰ to -7.1‰) corresponded to lower concentrations of soil components and Hg fractions[42].

The SOC content varies only slightly under sunlight, showing an initial decrease (0–75 days) followed by a slight increase (+ 0.8% at 75–150 days; Fig. 1B), whereas SIC shows an initial increase and then decrease (Fig. S1A). Such changes would be associated with, respectively, a gradual increase in DOC_{LS} and fluctuations in DOC_{CS} plus DIC_{LS+CS} (Fig. 1D-D and Fig. S1B-C)[7,8,14], and carbonate mineral neoformation by subsequent DIC_{LS+CS} uptake[67]. This finding is further supported by the net enrichment of δ^{13}C-STC and δ^{13}C-DOC in both labile and complexed state forms, due to the lighter[12]C export by SOC photorespiration. Notably, the gradual δ^{13}C-SOC depletion from −27.15‰ to −27.99‰ during the incubation period (Fig. 1E) would likely arise from the uptake of depleted CO_2 and/or DIC resulting from the photodegradation of DOC_{LS} and DOC_{CS}, which is further supported by the enrichment of the stable isotope values of δ^{13}C-DOC_{LS} and δ^{13}C-DOC_{CS} (Fig. 1G-H). This phenomenon consequently leads to continuous SOC photo-sequestration, which would offset photoinduced respiration, especially during the second half of the experiment. The substantial photoinduced C sequestration might be favored by the increased air moisture derived from intense precipitations (~ 240 mm), which occurred during the last 75 days of the experiment[23,73]. Remarkably, the simultaneous increase of photoinduced DOC_{LS} and δ^{13}C-DOC_{LS+CS} (Fig. 1C, G,H) suggests a continuous breakdown of SOC into relatively small, water-soluble compounds. Simultaneously, an increase in the fluorescence signals of humic acids and fulvic acids is observed in the water extracts (Figs. S1, S2 and Supplementary Table S1). Similar phenomena might be predicted on a global scale[7,8,17] in deforested lands, where sunlight-induced SOC transformation into DOM/DOC_{LS} in the top soil might accelerate soil erosion[15], decrease soil carbon storage[11,12], and cause land degradation[16] as global issues.

Most importantly, highly depleted δ^{13}C-DOC_{LS} values in three treatments (-29.00‰ to -28.68‰: Fig. 1D), when compared to the δ^{13}C-DOC_{CS} values (-26.94‰ to -26.37‰: Fig. 1D), likely indicate that the lighter DOC_{LS} would be exported into the surrounding surface and groundwater, while the highly enriched DOC_{CS} would remain in organo-minerals, contributing to C preservation and stabilization. In particular, this enriched carbon in DOC_{CS} may be kinetically favorable for the neoformation of organo-minerals. Furthermore, it has been reported that the highly depleted carbon in DOC_{LS} typically shows the higher molecular sizes and weights compared to DOC_{CS}[34]. This finding suggests that the relatively low molecular weights and sizes of organic substances, along with their enriched C content, may promote the neoformation of organo-minerals due to their lower steric hindrance.

Sulfur transformation

The net soil total sulfur (STS) increase with fluctuations (1.2–41.0%) under all conditions (sunlight, dark, and control at constant temperature, Fig. 1I) is the consequence of the fluctuation of soil organic sulfur plus sulfides/pyrites (SOS + S_n^{2-}) and of the different trends of SO_4^{2-}, depending on the occurrence of the LS or CS forms (Fig. 1I-L). These changes suggest that the occurrence of sulfide-dependent photosynthetic S sequestration[36] is taking place and is induced by, for instance, lichen-associated cyanobacterial-fungal symbioses through COS uptake[74] *via* irreversible redox reactions (e.g., $COS + H_2O \rightarrow 2H_2S + CO_2 \rightarrow CH_2O + 2S^o + H_2O$)[23,37,75,76]. Importantly, soils simultaneously uptake and produce COS and CO_2 or DIC, which occurs through the photochemical and microbial degradation of SOM[76,2,6,77–81] as well as redox reactions in oxygen-limited soils[82]. However, carbonic anhydrase activity in microbial communities for soil COS uptake is characterized by an enzyme-catalysed rate of COS hydrolysis, which ranges from 0.002 to 0.02 s^{-1} and is significantly faster on the shortest timescale compared to the enzyme-catalysed rate of CO_2-H_2O isotopic exchange (0.01 to 0.75 s^{-1})[83]. The rapid carbonic anhydrase activity in soil microorganisms is primarily responsible for COS uptake rather than CO_2.

Simultaneously, fluctuations in SOS + S_n^{2-} and $SO_4^{2-}{}_{CS}$ suggest the occurrence of sequestration-oxidation-reduction processes[31,36,37] consisting in S^o oxidation to SO_4^{2-} by soil fungi and bacteria[31], microbial SO_4^{2-} reduction to sulfides (S_n^{2-})[31], and S^{2-}/S_n^{2-} oxidation to SO_4^{2-} by Fe^{3+} and/or O_2[31]. Specifically, the eight electrons released from the reactions $S^{2-} \rightarrow S^O + 2e^-$ and $S^O \rightarrow SO_4^{2-} + 6e^-$[31] would generate H_2O_2 and $^{\bullet}OH$ radicals via $O_2^{\bullet-}$ intermediacy[43,84], which would contribute to mineralize the SOC or HS-bound clay and Fe minerals[14,30]. Overall, the simultaneous occurrence of the redox reactions $S^{2-} \rightleftharpoons S^o$ and $S^o \rightleftharpoons SO_4^{2-} \rightleftharpoons S^{2-}/S_2^{2-} \rightleftharpoons SO_4^{2-}$ would induce the concurrent sequestration of S and C, along with photochemical and microbial mineralization of SOC and HS-bound organo-minerals. Such S-mediated redox processes are further supported by the results from 100 soil samples collected across China, which showed that high soil S and SO_4^{2-} (both labile and mineral-bound) contents correlated well with low concentrations of various soil components, including Hg species in both solid and liquid phases across all soil types, and vice versa[42]. The detailed quantitative changes in SOS + S_n^{2-} and $SO_4^{2-}{}_{CS}$ are discussed in the supplementary note 1.

Differently, the linear $SO_4^{2-}{}_{LS}$ increase over time under all experimental conditions would primarily arise from the corresponding photo-microbial dissolution of SO_4^{2-}-containing minerals (e.g., clay)[24,27]. Remarkably, the higher $SO_4^{2-}{}_{LS}$ production in the dark, compared to sunlight and control at constant temperature, would attribute to enhanced dark/microbial mineral dissolution by intense microbial activities resulting from the wide-ranging day-night temperature variation (10–42 °C). The significant correlation of $SO_4^{2-}{}_{LS}$ with Ca_{LS}, Mg_{LS}, and Sr_{LS} (Fig. S4A-C; Table S2) suggests the formation of soluble sulfate forms that can be continuously exported into surface waters and groundwater.

Nitrogen transformation

The overall increase of soil total nitrogen (STN) under all conditions (Fig. 2A) likely reflects the increase of the different nitrogen (N) forms, including dissolved organic nitrogen (DON), NO_3^--N, and NH_4^+-N (Fig. 2) in LS samples, while the same forms fluctuate in CS samples, except for NH_4^+-N under sunlight. Simultaneously, stable isotopes of STN (δ^{15}N-STN) fluctuates and is depleted under sunlight exposure. An increase in STN would

derive from fresh N sequestration[38,65] by lichen-associated cyanobacterial-fungal symbioses[85]. Furthermore, the combination of STN increase and δ^{15}N-STN depletion under sunlight might suggest a continuous photoinduced uptake of lighter δ^{14}N-N_2O (from − 1.8‰ to -2.2‰)/N_2 (0‰)[1,86]. These processes are similar to the microbial depletion of δ^{15}N-STN occurring by biological uptake of lighter δ^{14}N-N_2O or N_2. Conversely, dark/microbial δ^{15}N-STN enrichment would probably arise from lighter N-losses in non-photosynthetic microbial processes[17].

Denitrification is the ending step of DON mineralization in both LS and CS forms under photoinduced and microbial conditions[1,17], which associates to NH_4^+-N_{LS+CS} and NO_3^--N_{LS+CS} production (Fig. 2). An increase of DON in both LS and CS forms has been reported at soil-microbe interfaces[65], due to continuous N uptake by *Geobacter* microbes[1], whereas its decrease would be related to the production of NH_4^+-N_{LS+CS} followed by photochemical and microbial nitrification-denitrification. Simultaneously, a strong correlation exists between DOC_{LS-S} and NH_3-N_{CS-S} (Fig. S4D; Table S2). A decrease in NO_3^--N is occasionally observed, which might involve N_2O emissions with δ^{15}N depletion[17]. Remarkably, the significantly higher export of NO_3-N_{LS} in the dark, compared to control and sunlight conditions, would arise from microbial mineralization of DON-bound DOC in both LS and CS forms (Figs. 1C and D and 2E). Furthermore, DON mineralization in both LS and CS forms mostly associates with amino functionalities in protein-like substances, resulting in complete degradation in LS forms and partial degradation in CS forms (Figs. S2, S3). Overall, the continuous N uptake is a key factor for subsequent DON mineralization, which leads to the export of dissolved N-nutrients into surrounding environments.

Metals transformations

Fe_{LS} levels decrease under sunlight over the periods of 0–30 days and 75–150 days (by 70.2% and 26.2%, respectively), but levels increase by 202% over a period of 30–75 days (Fig. 3). In contrast, Fe_{CS} levels decrease by 61.3% over the first 0–30 days and then gradually increase by 63.7–86.0% over the 30-50-150 day periods. A similar increasing and decreasing trend in both Fe_{LS} and Fe_{CS} levels is observed under both dark and control conditions across various time intervals (Fig. 3). These trends of increasing and decreasing Fe_{LS+CS} levels at specific time intervals under sunlight, dark, and control conditions (Fig. 3) suggest a dual behavior of Fe. A first process would entail the dissolution of HS-bound clay and Fe minerals[14], which concurrently promotes Fe redox properties by increasing the lability and solubility of Fe species[25]. The other process would involve photochemical and microbial neoformation of secondary minerals, e.g. DOM or HS-bound clay and Fe[14,24,30]. The latter components might be formed by organo-mineral complexation of HS functionalities with Fe *d*-orbitals *via* π–d interactions[30]. These processes would subsequently lead to SOC stabilization and sequestration by formation of soil organo-mineral complexes[13,14,40]. Similar dual roles of Fe have been observed in the transformation of C and N in previous studies[43,87–89]. In principle, a strong Fe^{3+} complexation behavior is typically due to stabilization of the π–d electron bonding system in Fe–DOM complexes through the donation of electrons from HS functionalities into the Fe d-orbitals[30] (Zhang et al. 2023) by the lower energy of the high-spin state, which has one electron in each of the five d-orbitals of $^{23}Fe^{3+}$ ($[Ar]^{18}3d^54s^0$), due to its greater electron-nucleus attraction[90]. This property allows Fe^{3+} ions to occur to a higher extent than other metals in

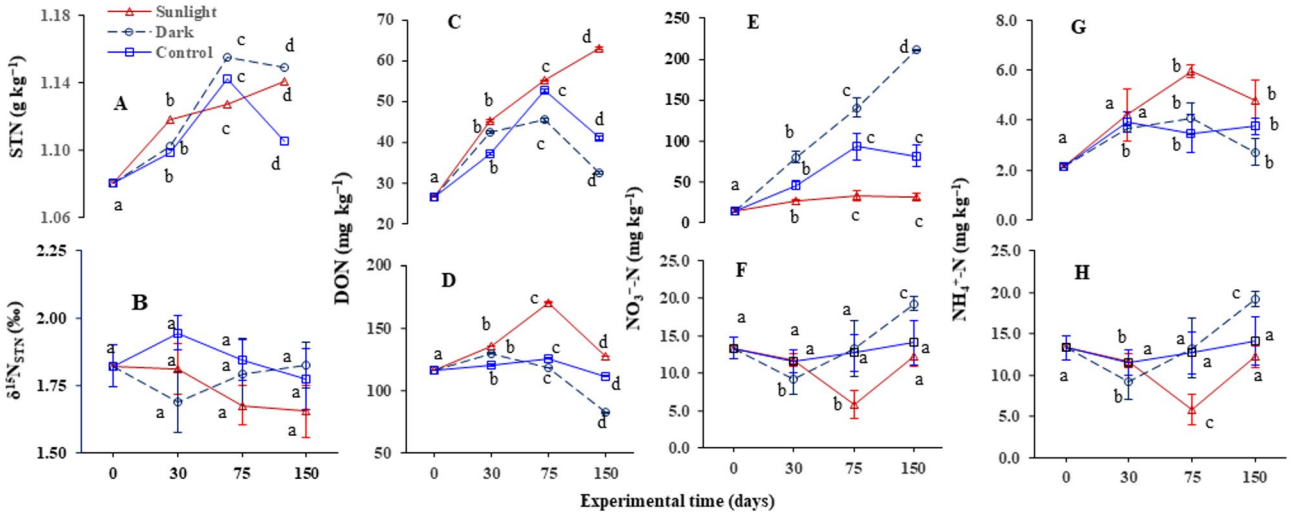

Fig. 2. Photoinduced (sunlight) and microbial (dark and control at constant temperature) changes of soil total nitrogen (STN, **A**); stable isotope of soil total nitrogen ($\delta^{15}N_{STN}$, **B**); dissolved organic nitrogen in labile state (LS) (DON_{LS}, **C**); DON in complexed state (CS) (DON_{CS}, **D**); NO_3^--N in LS (NO_3^--N_{LS}, **E**); NO_3^--N in CS (NO_3^--N_{CS}, **F**); NH_4^+-N in LS (NH_4^+-N_{LS}, **G**); and NH_4^+-N in CS (NH_4^+-N_{CS}, **H**) in extracts from soils subjected to sunlight, dark and control conditions measured at time 0 (original soil) and after 30, 75 and 150 consecutive experimental days. Error bars indicate the standard deviation among three replicates. The average values labeled with different letters (a, b, ab, c, d) at various time period (0, 30, 75, and 150 days) indicate significant differences ($p < 0.05$) among the three treated samples (sunlight, dark, and control at constant temperature), as determined by a one-way ANOVA.

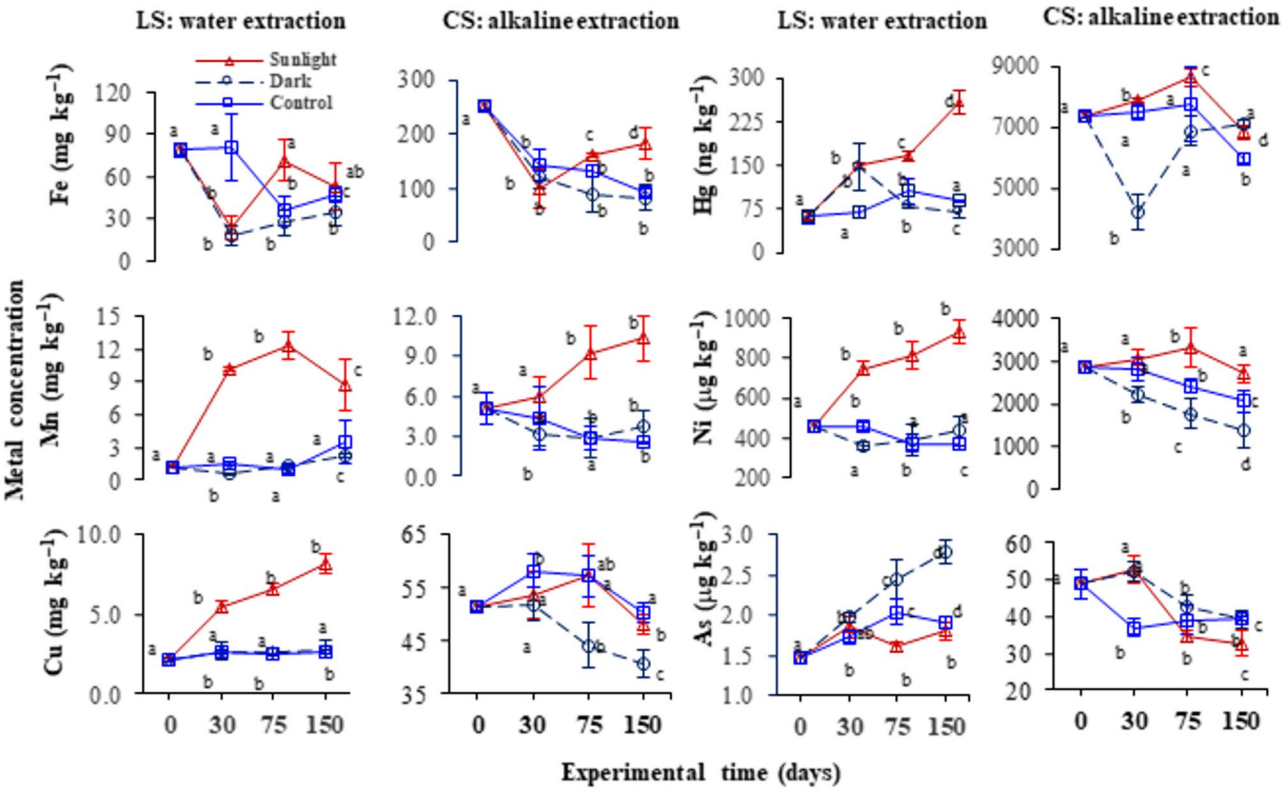

Fig. 3. Changes of Fe_{LS+CS}, Mn_{LS+CS}, Cu_{LS+CS}, Hg_{LS+CS}, Ni_{LS+CS} and As_{LS+CS} in water-extracts (labile state, LS) and alkali-extracts (complexed state, CS) from soils subjected to sunlight, dark and control conditions measured at time 0 (original soil) and after 30, 75 and 150 consecutive experimental days. Error bars indicate the standard deviation among three replicates. The average values labeled with different letters (a, b, ab, c, d) at various time period (0, 30, 75, and 150 days) indicate significant differences ($p < 0.05$) among the three treated samples (sunlight, dark, and control at constant temperature), as determined by a one-way ANOVA.

larger molecular DOM fractions[30,91]. Simultaneously, dark mineralization occurring at 10–42 °C due to various microbial activities[66,68] would lead to the highest SOC loss in dark conditions (by 10.8% decrease) compared to control samples (by 6.0% decrease) and to a decrease of organo-mineral stability, thereby enhancing surface soil erosion[15,16].

Furthermore, the trends (increase or decrease) of metals, both redox (Mn_{LS+CS}, Cu_{LS+CS}, Hg_{LS+CS}, Ni_{LS+CS}, As_{CS}, and U_{CS-S}) and non-redox ones (Al_{CS}, and Mg_{CS}) in specific timescales under sunlight (Fig. 3) suggests the occurrence of phenomena similar to those hypothesized for Fe, namely photoinduced and microbial change of redox properties together with increased lability or solubility and/or sequestration or neoformation of minerals and organo-minerals (see also supplementary Text 1–2)[13,14,24,25,30,40,43]. The latter phenomenon (neoformation of water-insoluble Fe minerals that include other metals as well) might also account for the observed U_{LS} transformation[24], which would also involve formation of U-phosphate minerals[92] (see also supplementary Text 2). Such U-bound mineral formation could be attributed to a significant decrease in U_{LS} over the first 0–30 days (by 39.0%) in dark samples, and over 30-75-150 days in both sunlight and control samples (by 16.0–40% and 8.4–42.0%, respectively). Additionally, a significant gradual increase in U_{CS} over the 0-30-75-150 day periods (44.0-66.0-84.7%) is observed in sunlight samples. In essence, U mineral neoformation would occur when U forms complexes with Fe oxyhydroxides through the hexavalent U species (UO_2^{2+}) (Fortier and Hayton 2010)[93,94], presumably via surface complexation or co-precipitation. Therefore, U_{LS} would be relatively less labile in dark and control conditions due to its strong complexation behavior in the form of water-insoluble U-complexes such as uraninite-UO_2/U-phosphate minerals, whereas U_{CS} shows a high photoinduced lability, but relatively low microbial lability in dark and control conditions.

Most importantly, Al_{CS} levels decrease over a period of 75–150 days under sunlight, dark, and control conditions (by 7.2%, 15.3%, and 9.6%, respectively), with the simultaneous decrease of Fe_{LS+CS}, Mn_{LS}, Cu_{CS}, Ni_{CS}, Mg_{CS}, As_{LS+CS}, and $SiO_3^{2-}{}_{CS}$, which would cause by the photochemical (sunlight samples) and microbial (dark and control samples) neoformation of Fe secondary silicate minerals (Figs. 3 and 4)[24,95,96]. These occur *via* the degradative by-products of HS components, as well as photosynthetically-derived SOC that generates HS components, which are detected under both sunlight and control conditions. These processes might be due to the high Al_{CS} occurrence that primarily promotes SOC stabilization and storage[13,97,98].

Remarkably, among the redox metals, Mn_{LS} levels undergo the most significant increase by 720–890% over the 0-30-75 day periods under sunlight (Fig. 3). This increase coincides with a rise in Mn_{CS} levels (by 54.0-

71.8%) over the 30-75-150 day periods. This phenomenon might be attributed to thermodynamic instability of Mn(III) due to its unfilled d-orbitals ($^{22}Mn^{3+}$ = [Ar]$^{18}3d^44s^0$), which is stable only in specific soluble organic complexes or minerals; and often disproportionates into soluble Mn(II) and insoluble Mn(IV)[12,99] (Tebo et al., 2004; Li et al. 2024; Wang et al. 2022) whereas Mn(II) is electronically more stable featuring five half-filled *d*-orbitals ($^{23}Mn^{2+}$ = [Ar]$^{18}3d^54s^0$). Moreover, the microbial (dark and control at constant temperature) Mn_{LS+CS} content is primarily regulated by SOC respiration and mineralization via S sequestration-redox reactions along with Mn^{2+} oxidation into Mn(III, IV), with neoformation of Mn minerals[99,100]. This process subsequently leads to lower Mn_{LS+CS} levels under both dark and control conditions, with the most significant decrease occurring over the first 0–30 days (by 38.5%) in dark conditions and over a period of 30–75 days (by 34.3%) in control samples. However, the simultaneous reductive dissolution of MnO_2 via redox processes ($S^o \rightleftharpoons SO_4^{2-} \rightleftharpoons S^{2-}/S_2^{2-} \rightleftharpoons SO_4^{2-}$) leads to increased $Mn^{2+}{}_{LS+CS}$ levels.

Similar trends as those observed in Mn_{LS+CS} and Fe_{CS} are also evident in Cu_{LS+CS} and Ni_{LS+CS} (Figs. 3 and 4), which leads to a continual export of Cu + Ni by photodissolution[14,96] and to the neoformation of HS-bound clay and Fe minerals[13,14,24]. A significant increase in Cu_{LS} levels is observed over the 0-30-75-150 day periods in sunlight samples, with increases of 156%, 20.4%, and 23.1%, respectively, and over the first 0–30 days (by 25.3%) in dark samples. Furthermore, Cu_{CS} levels significantly increase over 30–75 days (by 6.7%) in sunlight samples and over the first 0–30 days (by 13.0%) in control samples, while a significant decrease in Cu_{CS} levels is observed over the 30-75-150 day periods, with decreases of 15.1% and 8.1%, respectively, in dark samples. Ideally, the high Cu_{LS+CS} increase would be caused by photoreduction of Cu^{2+} to Cu^+ ($Cu^{2+} + e^- \Delta Cu^+$), i.e., a photoredox cycling[101] involving sulfur sequestration-redox cycle. Differently, Ni^{2+} undergoes one-electron redox processes to generate the Ni^+ ion that is highly reactive due to its outer-shell, one-electron unfilled *d*-orbital ($^{27}Ni^+$= [Ar]$^{18}3d^94s^0$). In this respect, Ni^+ is similar to Cu^+ and this determines the involvement of Ni^+ in a dinuclear Ni-bonding system (Ni-Ni) or Ni-organic compounds[102]. This hypothesis is further supported by a similar increasing trend in Ni_{LS} over the 0-30-75-150 day periods, with increases of 64.4%, 9.1%, and 14.0%, respectively, in sunlight samples, and a significant decrease in Ni_{CS} over the first 0–30 days in dark samples.

Remarkably, the high occurrence of Hg_{CS} (approximately, 25% of Hg_T) and its subsequent transformation/emission under all conditions leads to a decrease of Hg_T. For instance, up to 15% and 10% of Hg_T loss is observed under sunlight and dark conditions, respectively (Figs. 3 and 4). Such photochemical and/or microbial Hg_T losses would presumably occur by reduction of $Hg^{2+}{}_{CS}$ and $Hg^+{}_{CS}$ to highly volatile Hg^o[103]. Moreover, Hg_{LS} levels decrease over the 30-75-150 day periods (by 52.6% and 12.0%, respectively) in dark samples, while Hg_{CS} levels decrease over the first 0–30 days (by 46.0%) in dark conditions and over a period of 75–150 days in

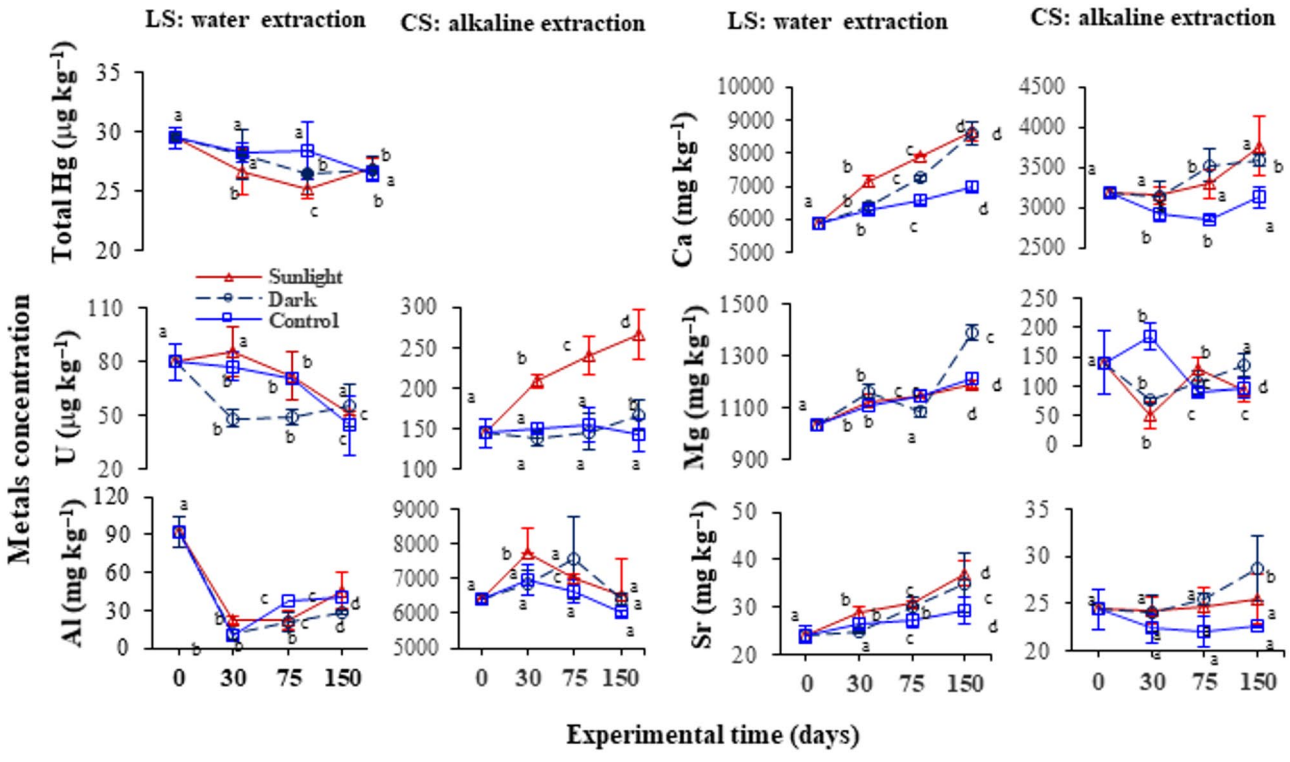

Fig. 4. Photoinduced and microbial changes of: total Hg, U_{LS+CS}, Al_{LS+CS}, Ca_{LS+CS}, Mg_{LS+CS} and Sr_{LS+CS} in water-extracts (LS) and alkali-extracts (CS) from soils subjected to sunlight, dark and control conditions measured at time 0 (original soil) and after 30, 75 and 150 consecutive experimental days. Error bars indicate the standard deviations among three replicates. The average values labeled with different letters (a, b, ab, c, d) at various time period (0, 30, 75, and 150 days) indicate significant differences ($p < 0.05$) among the three treated samples (sunlight, dark, and control at constant temperature), as determined by a one-way ANOVA.

sunlight and control samples (by 21.0% and 22.8%, respectively).Such Hg_{LS+CS} decrease under all conditions likely derives from HgS precipitation[26,104] triggered by the reduction of $SO_4^{2-}{}_{CS}$ to S^{2-} (Fig. 1). Simultaneously, Hg_{LS} levels increase (by 137%) over the first 0–30 days in dark samples and over the 0-30-75-150 day periods (by 139%, 11.2%, and 55.6%, respectively) in sunlight samples. This finding suggests that DOC_{LS+CS} containing Hg-DOM complexes would undergo mineralization, leading to a high export of Hg_{LS} and volatilization of Hg as Hg^0, thereby decreasing Hg_T over the first 0–30 days. Similarly, Hg_{CS} levels increase under dark conditions over a period of 30–75 days (by 62.7%) and over the 0-30-75 day periods (by 6.7% and 9.6%, respectively) in the sunlight samples, which would be ascribed either to the formation of Hg-thiol complexes with degradative HS functionalities[105] or to HgS precipitation by $SO_4^{2-}{}_{CS-D75}$ increase (3036%) via S^0 Δ $SO_4^{2-} \rightleftharpoons S^{2-} \rightleftharpoons S^0$ (Fig. 1). Additionally, an increase of Hg_{CS} would also suggest its sequestration by photosynthetically-derived SOC and/or HS functionalities, *via* Hg-thiols complexes (Fig. 4)[26,44], where newly-derived SOC and HS components are typically generated through photosynthesis in soil and sand environments[34,35]. The sequestration of Hg_{CS} via Hg-thiol complexes over a period of 30–75 days is accompanied by a simultaneous increase in SOS + S_n^{2-} (Fig. 1). Such processes result in a decrease in Hg_{LS} levels over 30–150 days and simultaneously involve the mineralization of DOC_{CS} under dark conditions (Figs. 3 and 4), which results in the reduction of DOM-Hg in Hg_{CS} to Hg^0[54], thereby decreasing Hg_T.

The consistently higher export of As_{LS} is observed in the dark over the 0-30-75-150 day periods (increase by 33.8%, 24.2%, and 14.2%, respectively) compared to sunlight samples (increase by 25.5%, decrease by 13.1%, and increase by 12.2%, respectively) and control samples (increase by 17.4% and 18.0%, and decrease by 6.2%, respectively) (Figs. 3 and 4). This phenomenon is attributed to the intense dissolution and respiration of HS-bound clay and Fe minerals, which are induced by the wide day-night temperature variation at T_{D10-42^oC} and are facilitated by diverse fungal-bacterial communities that are highly active under these conditions[66,68]. This process involves high SOC and/or DOC_{LS+CS} mineralization and absence of photosynthetically-derived SOC, which is further supported by a significant correlation between As_{LS} and SOC, or DOC_{LS}, or DOC_{CS} (Fig. S4E-F). This phenomenon might be a key worldwide signature for the increasingly high As export from soil due to mineral dissolution, a consequence of elevated temperatures induced by climate warming[28,29]. Differently, a decrease in As_{LS}, as previously mentioned, and As_{CS} over the 30-75-150 day periods in sunlight samples (by 34.4% and 5.7%, respectively) and dark samples (by 19.0%and 7.6%, respectively), as well as over the first 0–30 days (by 24.4%) in control samples would be associated with parallel decreases of Fe_{CS}, Mn_{CS}, Al_{CS}, and Mg_{CS} (Figs. 3). This phenomenon would imply the possible involvement of these elements in the neoformation of As-containing secondary minerals *via* either degradative HS byproducts or photosynthetically-derived SOC and HS components (Figs. 1 and 3)[43,106]. Ideally, electron transfer from the S sequestration-redox cycle would facilitate the oxidation of arsenite (AsO_3^{3-}) to arsenate (AsO_4^{3-})[107], leading to As sequestration or immobilization through the neoformation of secondary minerals involving Al_{CS}, Fe_{LS}, Mn_{LS}, and/or Mg_{CS}[24,40,106,108]. The outcome of these processes result in a decrease of these metals, including As_{LS+CS}, over the 30-75-150 day periods (Figs. 3 and 4). Remarkably, the higher electronic stability of AsO_4^{3-} ($^{28}As^{5+}$ = $[Ar]^{18}3d^{10}4s^04p^0$) compared to AsO_3^{3-} ($^{30}As^{3+}$ = $[Ar]^{18}3d^{10}4s^24p^0$) would result in the formation of more stable arsenate complexes with various Fe-oxides under alkaline conditions[109,110]. Ideally, the pH-dependent, negatively-charged arsenite/$H_2AsO_3^-$ plus arsenate/$H_2AsO_4^-$ would form strong complexes with the *d*-orbitals of Fe-minerals or oxides, and also with other metals[106,108,111], via π–d electron bonding systems similar to HS functionalities (e.g., COO^-)[30,41]. This would result in the simultaneous association of AsO_4^{3-}, AsO_3^{3-}, and HS components with various oxides or hydroxides of Fe and other metals[30,40,41,106,110,112].

Gradual increases in Ca_{LS}, Mg_{LS}, and Sr_{LS} over the 0-30-75-150 day periods under sunlight conditions (up to 47.8%, 15.3%, and 53.7%, respectively), dark conditions (up to 47.0%, 34.5%, and 45.0%, respectively), and control conditions (up to 19.6%, 17.1%, and 21.0%, respectively) are observed, with the sole exception of a Mg_{LS} decrease by 7.0% over a period of 30–75 days in dark samples. These findings would arise from lability and water-solubility of these cations that originate from the dissolution of the corresponding sulfate and clay minerals upon photochemical and microbial reactions[27,96,113–115]. In particular, Mg partially derives from the dissolution of chromite [$(Fe, Mg)Cr(III)_2O_4$][116]. Differently, Ca_{CS} and Sr_{CS} show a similar behavior, with slightly decreasing-increasing trends over the 0-30-75-150 day periods under sunlight, dark, and control conditions. Their relatively low input and/or transformation might be due both to their low occurrence in clay and silicate minerals together with the predominant occurrence of Si, Al, and Fe[96,113,115], and to the strong immobilization of Sr in clay minerals[117–119]. However, Mg_{CS} levels decrease over the first 0–30 days, both in sunlight and in dark (by 64.4% and 46.0%, respectively), over a period of 30–75 in control at constant temperature (by 50.6%) and over a period of 75–150 days in sunlight (by 26.8%) samples, while Mg_{CS} levels increase over the first 0–30 days in control at constant temperature (by 31.8%), over a period of 30–75 days in sunlight (by 157%) and over the 30-75-150 day periods in dark (by 39.0% and 27.8%, respectively) (Fig. 4). These phenomena presumably arise from the immobilized nature of Mg bound to various silicate interlayers[120] and also from its strong involvement in the neoformation or sequestration of clay minerals[24,30]. Therefore, the Mg_{CS} decrease under individual treatments would accompany the corresponding decrease of Al_{LS+CS}, Fe_{LS+CS}, Mn_{LS+CS}, Cu_{CS}, and Ni_{LS+CS}, due to formation of clay minerals through co-precipitation of degradative HS byproducts or photosynthetically-derived SOC[14,24,34,96,121],. Lastly, the Ca_{LS} and Mg_{LS} contents are 1.8- and 8.2-fold higher than, respectively, Ca_{CS} and Mg_{CS}, and nearly equivalent to Sr_{LS} with Sr_{CS}, which implies that environmental factors (e.g. sunlight and microbes) dissolve primarily various Ca, Mg, and Sr minerals whereas these elements occur preferentially in LS rather than CS-forms. In turn, this issue affects the lability and water-solubility of these three essential cations, constantly leaching them from soil to the surrounding ecosystems. The individual metal behaviors are discussed in the supplementary note 4.

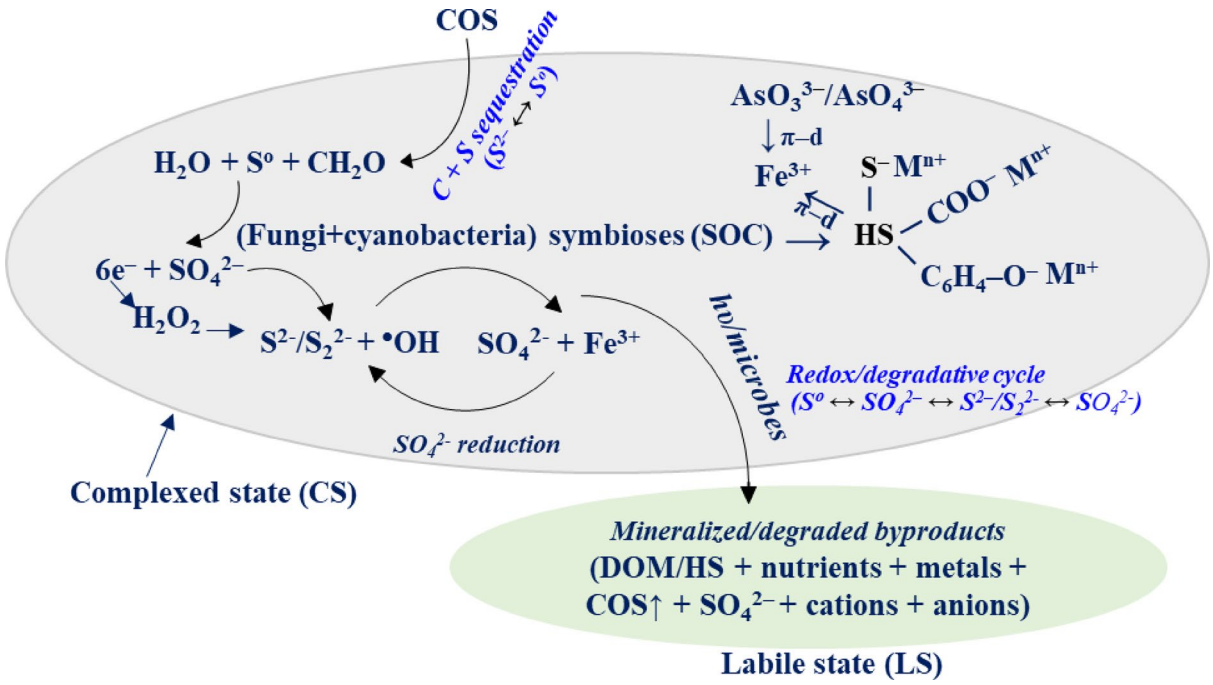

Fig. 5. A conceptual model of the simultaneous photosynthetic sulfur/COS acquisition or uptake via $S^{2-} \rightleftharpoons S^o$ and the subsequent oxidation-reduction via $S^o \rightleftharpoons SO_4^{2-} \rightleftharpoons S^{2-}/S_2^{2-} \rightleftharpoons SO_4^{2-}$ by fungi and cyanobacterial symbioses, showing the net S sequestration-redox in the corresponding transformation of soil organo-mineral components at mineral-microbe interfaces. These processes lead to dissolved-phase LS exports of dissolved organic matter (DOM)/humic substances (HS), nutrients, SO_4^{2-}, COS, cations and anions together with the subsequent sequestration/neoformation of minerals by uptake of various components of labile state (LS) and complexed states (CS) forms.

Discussion

Transformation and sequestration of soil organo-mineral components

The STS increase might be ascribed to lichen-associated cyanobacterial-fungal symbioses[74], as well as to non-symbiotic pathways[70–72]. In the former case, photosynthetic COS uptake for symbiotic growth[22,23,37] would occur at the microbe-mineral interface[14,65]. These processes would either increase or decrease the levels of $SO_4^{2-}{}_{CS}$ + SOS + S_n^{2-} (Figs. 1J, K,L), *via* sequential $S^{2-} \rightleftharpoons S^o$ and/or $S^o \rightleftharpoons SO_4^{2-} \rightleftharpoons S^{2-}/S_2^{2-} \rightleftharpoons SO_4^{2-}$ transformations[31,36]. The $S^{2-} \rightleftharpoons S^o$ plus $S^o \rightleftharpoons SO_4^{2-}$ conversion generates eight electrons, whereas high-valence labile redox metals coherently accept electrons to produce reduced low-valence forms, which can generate reactive oxygen species via Fenton/photo-Fenton reactions. The latter process would then induce SOC or DOC_{LS+CS} mineralization in minerals[14]. In return, the produced high-valence metals would cause neoformation or precipitation of minerals[13,24,25,40,103]. Such transformations involve the simultaneous dissolution and/or neoformation of HS-bound clay, and Fe minerals, through complexation/co-precipitation of HS or photosynthetically-derived SOC and HS[13,14,20,24,30]. These processes might also determine the export of water-soluble LS-forms (e.g. DOM, nutrients, and trace elements) to the surrounding ecosystems, which is depicted in a conceptual model (Fig. 5).

DIC_{LS} contents under sunlight appear to increase simultaneously with a net increase of DOM, HS fluorescence, nutrients, and redox/non-redox metals (Figs. 1, 2 and 3 and Figs. S3-S5), suggesting future increases of DIC in soils and waters under changing climatic conditions, which is a phenomenon similar to seawater carbonate dissolution. The export of various LS-components, particularly DOC, HA and FA, nutrients, redox and non-redox metals, and DIC, as well as CO_2, COS or H_2S emissions (Figs. 1 and 3 and Figs. S2-S5)[11,17,18] might occur in deforested land ecosystems due to enhanced exposure of soil to sunlight. Moreover, the initial DIC_{LS} decreasing rate under dark conditions over the first 0–30 days was 3.46 ± 1.15 mg $kg^{-1}day^{-1}$, which was higher than the rate observed for the subsequent 30-75-150 day periods (0.65 ± 0.56 and 1.14 ± 0.40 mg $kg^{-1}day^{-1}$, respectively). Similarly, the initial DIC_{CS} decreasing rate over the first 0–30 days was 4.74 ± 0.84 mg $kg^{-1}day^{-1}$, which was higher than for the rate observed for the subsequent 75–150 days (1.54 ± 0.16 mg $kg^{-1}day^{-1}$) (Fig. S1). In contrast, the relatively low decreasing rates of DIC_{LS} under control conditions over the 0-30-75 day periods (then compared to the dark samples) were 2.92 ± 0.73 and 0.49 ± 0.42 mg $kg^{-1}day^{-1}$, respectively. These phenomena under dark and control conditions would suggest the occurrence of two processes: (a) DIC uptake by photosynthetically-derived SOC[22,23,34,35,37], and/or silicate mineral weathering[67,122], both of which would be associated with the neoformation of clay, Fe or carbonate minerals; and (b) atmospheric emissions of DIC as CO_2[80,11,122].

Additionally, high soil respiration under dark conditions (10.0–42°C) is primarily responsible for high As export (Fig. 3)[14,28] and high SOC/HS mineralization. This process leads to a decrease in SOC sequestration and

its organo-mineral stability, thereby enhancing surface soil erosion[12,13]. The increasing temperatures associated with climate warming, particularly under dark conditions, significantly elevate the risks of As intrusion in both surface water and groundwater. Moreover, lichen-associated cyanobacterial-fungal symbioses would lead to neoformation of SOC- or HS-bound clay, Fe, and silicate minerals[14,24,25,30,40,43]. Such mineral formation would cause the sequestration of metals (e.g. Fe) and various anions, including nutrients (Fig. 2 and Fig. S5), while Hg decrease would result from the reduction of DOM-Hg complexes to volatile Hg^o[103,105], thereby increasing the risks of Hg exports into the surface water and groundwater, as well as its emissions into the atmosphere. Most importantly, the high Al_{CS} presence (approximately 70 times higher than Al_{LS} and 25 times higher than Fe_{CS} in untreated soil) suggests the fundamental role of clay or silicate minerals and/or organo-mineral complexes in the stabilization or storage of soil C[97,123].

Remarkably, microbial SOC mineralization, phototrophic carbon fixation, S redox processes, mineral neoformation, microbial biomass, and respiration processes have been discussed here based on the observed increases and decreases in solid-phase and liquid-phase soil components, along with references from previous studies, because direct evidence from this study is lacking. These soil biogeochemical processes should be emphasized in future research.

Conclusions

The assessment of photochemical and microbial interactions at 10–42 °C and 25 °C provides useful information on the simultaneous transformations of soil biogenic and non-biogenic elements derived from mineral dissolution and neoformation. In particular, mineral dissolution can lead to the release of water-soluble species, including DOM, DIC, HS components, nutrients, and both redox and non-redox metals/elements, such as carcinogenic As and Hg, into the surrounding environments-namely surface water, groundwater, and the atmosphere. The key findings about the various features of mineralization-sequestration of clay, and Fe mineral components are summarized below. First, among redox metals, Fe always plays a dual role, i.e., organo-mineral complexation[13,24,43] due to its five half-filled Fe d-orbitals[30] and redox behavior[14,25].

Second, the reduction of DOM-Hg in Hg_{CS} to volatile Hg^o[103,124] would lead to a net Hg decrease under sunlight, dark and control conditions over the 0-30-75-150 day periods (a decrease by 9.7–14.8%, 4.98–10.2%, and 3.52–10.4%, respectively), which would indicate the continuous Hg^o emission from degraded and dry-affected lands. This process poses significant human health risks, either directly or through microbial food webs.

Third, the consistently higher As_{LS} export in dark conditions over the 0-30-75-150 day periods (6.6–55.2% and 14.0-46.1%, respectively) compared to sunlight and control conditions (Fig. 3) would be due to a continuous and high dissolution or respiration of HS-bound clay and Fe minerals induced by the wide day-night temperature variation at T_{D10-42^oC} and operated by diverse fungal-bacterial communities that are highly active in these conditions[66,68,125]. This process involves high SOC and DOC_{LS+CS} mineralization and absence of photosynthetically-derived SOC, which might be key signatures for the increasingly high As export from soil caused by mineral dissolution worldwide as a consequence of increased temperatures[28,29,40] due to climate warming. This process also presents significant risks to human health, either directly or through microbial food webs.

Fourth, the high Al_{CS} presence, approximately 70-fold higher than Al_{LS} and 25-fold higher than Fe_{CS} in untreated soil, would suggest the fundamental role of clay or silicate minerals and/or organo-mineral complexes in stabilization and storage of soil carbon[14,97,126,127].

Fifth, photorespiration appears to increase DIC_{LS} concentration at the same time as it causes a net increase of DOM, HS fluorescence, nutrients, redox and non-redox elements (Figs. 1, 2, 3 and 4 and Figs. S3-S5). These findings suggest a potential increase in the dissolution behavior of DIC in soils and waters under changing climatic conditions, a phenomenon akin to seawater carbonate dissolution.

Sixth, the photosynthetic uptake of C[17,31–34], N[1,2,37,38,134], S[35,36], and various other elements[4,24,25,30,40–42] is a key process driving increases in SOC levels through photosynthetically-derived EPS or HS components produced by soil microorganism[21,22,34,35,42,43,73,133]. This process, i.e., increases in SOC, counterbalances simultaneous degradative losses of EPS and other soil components through photosynthetically driven, sulfur-mediated sequestration-redox processes[14,31,134,135]. Increasing SOC persists in soils through organo-mineral neoformation involving EPS or HS components, which help maintain steady-state SOC levels, while degradative loses of labile soil components may continuously be exported, leached, or emitted from terrestrial soils into surrounding environments.

Seven, fluorescence studies of HS components and other soil components[54] have confirmed that the extraction time used for two sequential water extractions (6 h + 1 h), followed by two sequential extractions (3 h + 3 h), is essential for the effective dissolution of both water- and alkali-extractable soil components. Reducing the time may result in incomplete dissolution, while extending it unnecessarily might partially alter discrete or functionally distinct components. Using this extraction procedure, the total SOC values ranged from 1.41 to 5.89% in water extracts and from 5.83 to 9.52% in alkali extracts from both raw and treated soils. These results demonstrate a substantial yield of SOC, which is critical for understanding the biogeochemical characteristics, functions, and influencing factors of various soils and sands[30,34,35,42]. This study, along with recent publications[30,34,35,42], highlights the effectiveness and potential of this extraction technique.

Finally, the results of the experiments conducted on soil samples within the day-night experimental temperature range (10–42 °C) under both sunlight and dark conditions, in comparison with the control at constant temperature (25 °C), are reasonably expected to enhance our understanding of certain aspects of ongoing climate warming processes. In particular, sunlight-induced exports of redox metals and DOM are expected to affect soil worldwide by increasing erosion and will also degrade the soil and water ecosystem and their services, which remain a crucial issue of immense global ecological and economic significance.

Materials and methods

Samples

Approximately 5 kg soil, classified as haplic luvisol, free of plant litter and debris, were collected in black airtight polypropylene bags from the A-horizon (0–30 cm) of the Panshan deciduous forest floor, Tianjin, China (N40°00′990″, E117°15′804″). The forest site is located very close to a stream between two mountains and is covered mostly by a deciduous man-made forest densely populated by Pine trees[21]. The collected soil in the sampling site is undisturbed and remains under natural conditions, as reported elsewhere[21]. Soil samples were then 2-mm sieved and mixed homogeneously, to generate a sample that is spatially representative at the field scale.

Experimental protocols

Three experimental protocols, i.e., sunlight, dark, and control at constant temperature were conducted on three aliquots of about 50 g each of the homogeneously mixed 2-mm sieved soil during the warm season, from May 5th to October 1st, 2018, for 150 days. In particular, the 'sunlight' experiment aimed at evaluating the photorespiration and/or photodegradation with photosynthetically-derived SOC sequestration of soil organo-mineral components, and was conducted on soil samples placed in 500-mL quartz bottles. Notably, the quartz bottle measures exactly 19.0 cm in length and 7.5 cm in width, with a mouth opening of ~ 4.3 cm and a neck length of approximately 4.0 cm. Each bottle's mouth was covered by parafilm with small holes to allow for oxygen exchange, and the bottles were placed under natural sunlight conditions on the roof of a building of Tianjin University, Tianjin, China. Quartz bottles were used to avoid the blockage of ultraviolet (UV) wavelengths by glass and were placed on a strong support at opposite angles of 45 degrees, with the mouth positioned downward to avoid the effect of any precipitation or contamination, taking advantage of their long-necked designed.

The 'dark' experiment, which aimed at evaluating the microbial respiration and/or biodegradation in the same system, was conducted on soil samples put in 500-mL glass bottles and placed in the same site indicated above, with the mouth loosely bound to allow for limited gas exchange and covered with aluminum foil to avoid sunlight exposure. In particular, the 500 mL amber bottles were specifically designed in consultation with company representatives and ordered for this experimental analysis. These bottles feature a brown color and a wide mouth, while the cap-type stoppers are made of light-resistant black plastic. Notably, the glass bottle measures exactly 14.0 cm in length and 8.0 cm in width, with a mouth opening of ~ 4.3 cm and a neck length of approximately 2.0 cm. Aluminum foil does not cover the caps/mouth of the bottles and is loosely bound to allow for adequate air circulation; therefore, heat retention does not occur in the experimental bottles. In these conditions the soil samples were subject to the effects of day-night temperature differences that can activate different fungi-bacteria, which are primarily responsible for respiration influenced by climatic change[128]. Finally, the 'control at constant temperature' experiment aimed at assessing the differences in microbial responses at a fixed temperature compared to day-night cycles, and was conducted in the laboratory. The soil samples were placed in identical 500-mL brown amber glass bottles and kept in a thermostat maintained at a constant temperature of 25°C. The plastic caps were loosely sealed to facilitate air exchange with the soil samples in the thermostat. All 'control at constant temperature' bottles were removed from the thermostat, and the caps were completely opened for a moment to allow for adequate air circulation during the middle stage of each experimental interval before being placed back in the thermostat. Three replicate samples under sunlight, dark, and control conditions are applied for each time point: 0 days, 30 days, 75 days, and 150 days of incubation.

In summary, a 'dark' sample or experiment can be defined as a soil that has been subjected to subsequent microbial transformation (mineralization and sequestration) of soil organic matter (SOM), and has experienced fluctuations in temperature between day and night. These conditions can be compared to natural soil environments influenced by dark and microbial activities. In contrast, a 'control at constant temperature' sample or experiment refers to a soil that has also been subjected to subsequent microbial transformation (mineralization and sequestration), but is maintained at a constant temperature of 25°C under controlled microbial and dark conditions in a thermostat, which allows for a comparison of its transformations with those of dark samples.

A 'sunlight' sample or experiment can be defined as a soil that has been subjected to subsequent photochemical transformation (mineralization and sequestration) of SOM, while being exposed to sunlight during the daytime. These conditions can be compared to natural soil environments affected by daytime sunlight exposure on deforested land, as well as on various surface soils. The objective of this 'sunlight' experiment is to evaluate the photorespiration and/or photodegradation in relation to photosynthetically-derived SOC sequestration at the soil surface.

During the 'sunlight' and 'dark' experiments, the highest air temperature recorded was 41.8 °C in July 2018, based on diurnal temperature data collected near the experimental site[136]. The lowest experimental temperature, 10 °C, was obtained from monthly meteorological data recorded in Tianjin in September. Therefore, the air temperature ranged from 10.0 to 41.8 °C with significant monthly variations from May to September, with June, July, and August as the hottest months on average[137] (Source: www.tianqi.com). The solar intensity during the experimental period was very variable as well, ranging from 231.2 Wh m^{-2} hr^{-1} in September to 262.4 Wh m^{-2} hr^{-1} in June[127]. Precipitation was also unevenly distributed, with the highest values in July (232 mm) and August (~ 190 mm) and the lowest in September (~ 8 mm)[128]. Note that soil samples were not directly exposed to rain, but humid air could come in contact with the studied soils. Water was not added to the samples because the experiments were focused on the impact of dry conditions under sunlight and temperature variations on the surface soil. However, an increased humidity during the rainy seasons was contributed in the experimental protocols. To prevent the direct reaching of rainwater to sunlight samples, the corresponding bottles are specifically configured as previously described. Notably, the direct moisture influence on the experimental soils are mitigated by using parafilm with small holes to cover the mouth of each bottle. This design also facilitates air exchange within the experimental bottles, as previously mentioned. In contrast, dark and control bottles are

loosely sealed with plastic caps as mentioned previously, allowing air moisture to remain in a saturation state within the treated soil samples.

The pH of raw forest soil is measured at 7.20 ± 0.03 and it typically increases across all three treatments, varying from 7.29 ± 0.07 to 7.38 ± 0.07 in sunlight conditions, from 7.25 ± 0.09 to 7.32 ± 0.02 in dark conditions, and from 7.28 ± 0.12 to 7.40 ± 0.03 in control conditions (Fig. S1D). Similarly, the electric conductivity (EC) of raw forest soil is measured at 105 µS/cm, and it typically increases across all three treatments, showing the highest increase of 51.3% in the dark, 29.4% in sunlight, and 22.8% in control samples (Fig. S1E).

Three soil sample replicates were collected consecutively after 30, 75, and 150 days, oven-dried at 40 °C for 24 h, and then pestle-ground at a < 0.2 mm size in a mortar for further analyses.

Extraction protocol

The organo-mineral components were isolated from soil samples by extraction with water followed by a 0.1 M NaOH solution. The water extract (W_e) was obtained by a number of subsequent steps (Fig. S6). In the first step, ultrapure water (18.2 MΩ·cm, Mill-Q, Millipore) was added to the ground and 0.2-mm-sieved soil sample at a soil/water ratio of 1:10, the mixture was vortexed for 1 min in closed 500-mL brown bottles and then shaken for 6 h at 25 °C. The mixture was then centrifuged for 20 min at 4000 rpm using a Thermo Fisher Scientific SORVALL ST 16 centrifuge to remove suspended solids. The supernatant solution was then filtered through a 0.45-µm membrane filter (GF/F type, Shanghai Xin Ya Purification Equipment Co. Ltd, China), whereas the remaining solid residue was extracted again with fresh ultrapure water for 1 h, and the procedure described above applied again to obtain another supernatant solution that was mixed with the previous one and stored in freezer at − 20 °C until further processing.

The alkaline extract (A_e) under N_2 was obtained by adding a 0.1 M NaOH solution to the corresponding W_e soil residue at a soil residue/alkaline solution ratio of 1:10, shaking the mixture for 3 h at 25 °C, and then centrifuging it as described above. The supernatant solution was filtered through a 0.45-µm membrane filter (polytetrafluoroethylene membrane, PTFE, Shanghai Xin Ya Purification Equipment Co. Ltd, China), whereas the remaining solid residue was extracted again with a fresh alkaline solution for 3 h and, after applying again the above procedure, a further supernatant solution was obtained that was mixed with the previous one and stored in freezer at − 20 °C until further processing. The W_e and A_e samples provide the water-soluble labile state (LS) and water-insoluble complexed state (CS) fractions of soil organo-mineral components[20,21]. They are expected to provide relevant information on the biogeochemical phenomena, mechanisms, and origin of soil organo-mineral components, DOM, HS, nutrients, and metals. Based on the extraction yield and timing, the contributions of W_e (water extracts) and A_e (alkali extracts) to the total SOC in raw soils were approximately 1.86% and 8.06%, respectively. These contributions were relatively higher for sunlight-exposed samples, ranging from 3.63% to 5.89% for water extracts and 8.20% to 9.52% for alkali extracts, and relatively lower for microbial (dark and control at constant temperature) samples, ranging from 1.41% to 1.80% and 5.83% to 8.79%, respectively.

Sample analyses

Soil total carbon (STC), soil organic carbon (SOC), N, and S contents were measured by a Vario EL Cube Elemental Analyzer (Elementar VarioEL III, Germany) as reported previously[21], on approximately 20 mg aliquots of dried, ground, and homogenized soil sample contained in a clean, carbon-free, pre-combusted tin boat placed on an autosampler rack assembly. In the case of SOC measurement, the dried, ground, and homogenized soil samples were pretreated with 1 M HCl in a vial to remove carbonates[52]. Sulfanilamide was used as standard after every 10 measurements.

The stable isotopes ^{13}C and ^{15}N were analyzed on 2.0 mg and 30.0 mg, respectively, of dried soil samples contained in tin boats placed on the autosampler rack assembly of the Elemental Analyser (Flash 2000 HT) interfaced with Stable Carbon Isotope Ratio Mass Spectrometer (MAT 253 Plus, ThermoFisher, USA). The IAEA-600 Caffeine was used as the ^{13}C standard, whereas for ^{15}N measurements, both IAEA-600 Caffeine and USGS 40 plus 41 L-Glutamic Acid were used as standards.

The dissolved organic carbon (DOC) content in soil solutions was measured in triplicate using an Aurora combustion total organic carbon (TOC) analyzer (OI Analytical Aurora, Model 1030, USA), according to a procedure reported previously[21]. Soil particle sizes were determined by the hydrometer method using a Master sizer 3000 (Malvern), with soil classification based on the WRB Texture Classes, i.e., sand (63–2000 µm), silt (2–63 µm), and clay (< 2 µm). The pH and electric conductivity (EC) were determined in suspensions at a soil/water ratio of 1:2.5 using a pH meter (Multi 3630 IDS, Germany).

The nutrients NO_3^-, NH_4^+, total N (TN), PO_4^{3-}, total phosphorus (TP), and Si were measured in the soil solutions colorimetrically using an automated continuous flow analyzer (Skalar San^{++} System, Skalar Analytical B.V., The Netherlands). The SO_4^{2-} concentrations were measured using a Thermo Fisher SCIENTIFIC DIONEX ICS 5000 + USA ion chromatograph in controlled environment (23°C and 40% humidity). Soil organic sulfur plus sulfides/pyrites ($SOS + S_n^{2-}$) were estimated from the equation: $SOS + S_n^{2-} = STS - S_{LS} - S_{CS}$, where STS is the soil total sulfur, while S_{LS} and S_{CS} are the S content in $SO_4^{2-}{}_{LS}$ and $SO_4^{2-}{}_{CS}$, respectively. The S content in $SO_4^{2-}{}_{LS}$ and $SO_4^{2-}{}_{CS}$ was calculated as: $A \times (S_{MW}/B_{MW})$, where A is the SO_4^{2-} concentration, S_{MW} is the atomic weight of S, and B_{MW} is the molecular weight of SO_4^{2-}.

The trace metals/elements (Ca, Mg, Fe, Al, and Si) were analyzed on digested soil samples by inductively coupled plasma optical emission spectroscopy (ICP-OES, Agilent 5110) and the other metals (Mn, Cu, Ni, As, Sr, and U) by inductively coupled plasma mass spectrometry (ICP-MS, Agilent 7900). Briefly, approximately 0.25 g of soil were treated with a solution of 3 mL ultrapure 40% HCl and 9 mL ultrapure 80% HNO_3 in a Teflon vessel and then digested in a Microwave Digestion System (MARS 6, CEM, USA), according to the EPA method 3051 A. Digestion was continued until a few drops of solution remained in the digested soil residue which was then transferred to a Teflon bottle and finally diluted to 50 mL with 3% HNO_3. The extracted solution was then

filtered using a syringe filter (0.45 µm, PTFE, Pall Corporation, USA) and stored in 50 mL polypropylene bottles. Blank (only acid) and standard samples were prepared using a similar procedure. The standard sample provided by Agilent Technologies was used to make the calibration of the standard solution. Quality assurance and quality control procedures were ensured by using standard reference materials supplied by Agilent Technologies. Owing to the high sensitivity of ICP-MS, ultra-high-purity grade HNO_3 was used as the blank. One standard was measured with an interval of every ten samples and a solvent blank set with an interval of each batch sample. Average recoveries of standard reference metals ranged from 95% to 105% with a test precision within 5%. The entire system was controlled by the MassHunter Workstation 4.4 software (Agilent Technologies).

The Hg concentrations in W_e and A_e samples were measured by a Cold Vapor Atomic Fluorescence Spectroscopy (CVAFS) Analyzer (Tekran 2600, Tekran Instruments Corporation, Knowville, TN, USA) according to the EPA method 1631E. The samples were processed in a dark cold room at 4 °C and oxidized with 40% (v/v) of $2HNO_3$/1HCl with 1% (v/v) solution of 0.2 M BrCl[139]. The total Hg in soil was measured on soil samples ground in an agate mortar and sieved at a size < 0.075 mm, with precautions taken to avoid cross-contamination of samples, using a Lumex RA915F Mercury Analyzer equipped with a PYRO-915 + unit and Zeeman Atomic Absorption Spectrometry[139]. In this method, Hg in the soil samples was released as Hg(0) vapor during pyrolysis at approximately 750 °C and subsequently measured using Zeeman Atomic Absorption Spectrometry. Prior to analysis, the instrument was calibrated by certified reference materials (CRMs) in the range of 20 to 50 ng of Hg. The values of CRMs were within ± 5% of their certified values.

Absorption spectra of solutions were recorded from 200 to 800 nm at 1-nm interval using a quartz cell of 1-cm path length by a UV-VIS spectrophotometer (UV-2401PC, Shimadzu). Fluorescence excitation-emission matrix (EEM) spectra were acquired by a fluorescence spectrophotometer F-7000, Hitachi (Japan) using a procedure reported previously[21]. Ultrapure water (18.2 MΩ cm) was used as the blank and measured every ten samples, to check for the performance of the instrument and ensure data quality. The pure water EEM data were subtracted from the corresponding sample EEM spectra. A 10-µgL^{-1} quinine sulphate (QS) solution in 0.01 N H_2SO_4 was used for fluorescence normalization. The fluorescence intensities of all samples were calibrated using the intensity of the QS (1 µg L^{-1} = 1 QS unit, QSU) peak at Ex/Em = 350/450 nm[21]. To avoid inner-filter effects and fluorescence quenching, the sample solutions were diluted based on the initially measured DOC concentration and then EEM was measured. The fluorescence intensity of each peak was rechecked and corrected using a common absorbance-based approach[129]. Preprocessed EEM data were analyzed by the parallel factor (PARAFAC) model using the N-way Toolbox for MATLAB[130] as described elsewhere[131]. First, Rayleigh and Raman peaks, as well as an ultrapure water blank, were subtracted from the measured EEM spectra using a home-made Excel program. Second, in order to avoid the mixing of fluorescent components of different soil samples that could produce artifacts[131], PARAFAC analysis was performed individually on each soil sample. Finally, non-negative constraints were applied to the PARAFAC model. The detailed procedure of using PARAFAC modeling of EEM spectra was reported previously[21]. All statistical data analysis was performed by multivariate analysis and descriptive statistics using the Origin 2018 version 9.5 (https://www.originlab.com).

Definitions

LS Labile state. Labile state refers to the labile forms of water-soluble soil components found in water-extracts obtained by a specific time-dependent extraction process using ultrapure water from soil and are influenced by existing environmental conditions such as moisture, temperature, redox properties, mineral matrix, and microbial activities in the soils. These LS soil components are typically leaching from soils into the surrounding surface and groundwater via water infiltration or rainwater runoff.

CS Complexed state. Complexed state refers to the organo-mineral forms of soil components that remain complexed with soil minerals and are insoluble in water. These organo-mineral components can only be dissolved and extracted using an alkali solution (O.1 M NaOH) through a specific time-dependent extraction method applied to the soil residue left after water extraction. CS soil components typically remain in the soils during water infiltration or rainwater runoff. These fractions, however, are operationally defined and may not correspond exactly to discrete or functionally distinct biogeochemical pools in natural soils.

Data availability

The authors declare that data is provided within the manuscript or supplementary information files.

Received: 16 January 2025; Accepted: 15 September 2025
Published online: 21 October 2025

References

1. Barron, V. et al. Photochemical emission and fixation of nox gases in soils. *Sci. Total Environ.* **702**, 134982 (2020).
2. Whelan, M. E. & Rhew, R. C. Carbonyl sulfide produced by abiotic thermal and photodegradation of soil organic matter from wheat field substrate. *J. Geophys. Res. Biogeosci.*. **120**, 54–62 (2015).
3. Yang, W., Yuan, H., Han, C., Yang, H. & Xue, X. Photochemical emissions of HONO, NO2 and NO from the soil surface under simulated sunlight. *Atmos. Environ.* **234**, 117596 (2020).
4. Jung, H. et al. Photocatalytic oxidation of dissolved Mn (II) on natural iron oxide minerals. *Geochim. Cosmochim. Acta.* **312**, 343–356 (2021).
5. Crowther, T. W. et al. Quantifying global soil carbon losses in response to warming. *Nature* **540**, 104–108 (2016).
6. Bond-Lamberty, B. & Thomson, A. Temperature-associated increases in the global soil respiration record. *Nature* **464**, 579–582 (2010).
7. Davidson, E. A. & Janssens, I. A. Temperature sensitivity of soil carbon decomposition and feedbacks to climate change. *Nature* **440**, 165–173 (2006).

8. Drake, T. W. et al. Mobilization of aged and biolabile soil carbon by tropical deforestation. *Nat Geosci.* **12**, (2019).
9. Dorrepaal, E. et al. Carbon respiration from subsurface peat accelerated by climate warming in the Subarctic. *Nature* **460**, (2009).
10. Fang, C., Smith, P., Moncrieff, J. B. & Smith, J. U. Similar response of labile and resistant soil organic matter pools to changes in temperature. *Nature* **433**, 57–59 (2005).
11. Melillo, J. M. et al. Long-term pattern and magnitude of soil carbon feedback to the climate system in a warming world. *Science (80-)*. **358**, 101–105 (2017).
12. Li, Y. et al. Deforestation-induced climate change reduces carbon storage in remaining tropical forests. *Nat. Commun.* **13**, 1964 (2022).
13. Hemingway, J. D. et al. Mineral protection regulates long-term global preservation of natural organic carbon. *Nature* **570**, 228–231 (2019).
14. Kleber, M. et al. Dynamic interactions at the mineral-organic matter interface. *Nat. Rev. Earth Environ.* **2**, 402–421 (2021).
15. Galy, V., Peucker-Ehrenbrink, B. & Eglinton, T. Global carbon export from the terrestrial biosphere controlled by erosion. *Nature* **521**, 204–207 (2015).
16. Lal, R. Restoring soil quality to mitigate soil degradation. *Sustainability* **7**, 5875–5895 (2015).
17. Lerch, T. Z., Nunan, N., Dignac, M. F., Chenu, C. & Mariotti, A. Variations in microbial isotopic fractionation during soil organic matter decomposition. *Biogeochemistry* **106**, 5–21 (2011).
18. Maseyk, K. et al. Sources and sinks of carbonyl sulfide in an agricultural field in the Southern great plains. *Proc. Natl. Acad. Sci. U S A*. **111**, 9064–9069 (2014).
19. Doane, T. A. Photochemical emission from soil as a source of atmospheric CO2. *ACS Earth Sp Chem*. **9**, 207–210 (2025).
20. Lehmann, J. & Kleber, M. The contentious nature of soil organic matter. *Nature* **528**, 60–68 (2015).
21. Mohinuzzaman, M. et al. Insights into solubility of soil humic substances and their Fl Uorescence characterisation in three characteristic soils. *Sci. Total Environ.* **720**, 137395 (2020).
22. Loron, C. C. et al. Early fungi from the proterozoic era in Arctic Canada. *Nature* **570**, 232–235 (2019).
23. Heckman, D. S. et al. Molecular evidence for the early colonization of land by fungi and plants. *Sci. (80-)*. **293**, 1129–1133 (2001).
24. Khan, A. I. & O'Hare, D. Intercalation chemistry of layered double hydroxides: recent developments and applications. *J. Mater. Chem.* **12**, 3191–3198 (2002).
25. Chen, C., Hall, S. J., Coward, E. & Thompson, A. Iron-mediated organic matter decomposition in humid soils can counteract protection. *Nat. Commun.* **11**, 1–13 (2020).
26. Zhou, J., Obrist, D., Dastoor, A., Jiskra, M. & Ryjkov, A. Vegetation uptake of mercury and impacts on global cycling. *Nat. Rev. Earth Environ.* **2**, 269–284 (2021).
27. Krumgalza, B. S. Temperature dependence of mineral solubility in Water. Part 3. alkaline and alkaline Earth sulfates. *J Phys. Chem. Ref. Data* **47**, (2018).
28. Islam, F. S. et al. Role of metal-reducing bacteria in arsenic release from Bengal delta sediments. *Nature* **430**, 68–71 (2004).
29. Nickson, R. et al. Arsenic poisoning of Bangladesh groundwater. *Nature* **395**, 338 (1998).
30. Zhang, J. et al. Isolation of dissolved organic matter from aqueous solution by precipitation with FeCl3: mechanisms and significance in environmental perspectives. *Sci. Rep.* **13**, 1–15 (2023).
31. Lovley, D. R. Bug juice: harvesting electricity with microorganisms. *Nat. Rev. Microbiol.* **4**, 497–508 (2006).
32. Daval, D. Carbon dioxide sequestration through silicate degradation and carbon mineralisation: promises and uncertainties. *Npj Mater. Degrad.* **2**, 11 (2018).
33. Qin, C. et al. Vertical variations of soil carbon under different land uses in a karst critical zone observatory (CZO), SW China. *Geoderma* **412**, 115741 (2022).
34. Yang, X. et al. Mineral States and sequestration processes involving soil biogenic components in various soils and desert sands of inner Mongolia. *Sci. Rep.* **14**, 28530 (2024).
35. Gao, X. et al. Sulfur-mediated transformation, export and mineral complexation of organic and inorganic C, N, P and Si in dryland soils. *Sci. Rep.* **15**, 1–21 (2025).
36. Kelly, B. et al. Sulfur sequestration promotes multicellularity during nutrient limitation. *Nature* **591**, 471–476 (2021).
37. Cohen, Y., Jorgensen, B. B., PADAN, E. & Shilo, M. Sulphide-dependent anoxygenic photosynthesis in the Cyanobacterium oscillatoria limnetica. *Nature* **257**, 489–492 (1975).
38. Levican, G., Ugalde, J. A., Ehrenfeld, N., Maass, A. & Parada, P. Comparative genomic analysis of carbon and nitrogen assimilation mechanisms in three Indigenous bioleaching bacteria: predictions and validations. *BMC Genom.* **9**, 1–19 (2008).
39. Yang, W. et al. Heterogeneous photochemical uptake of NO2 on the soil surface as an important ground-level HONO source. *Environ. Pollut.* **271**, 116289 (2021).
40. Moore, O. et al. The role of electron donors in arsenic-release by redox-transformation of iron oxide minerals - A review. *Chem Geol* 121322 (2023).
41. Couture, R. M. et al. Sorption of arsenite, arsenate, and thioarsenates to iron oxides and iron sulfides: a kinetic and spectroscopic investigation. *Environ. Sci. Technol.* **47**, 5652–5659 (2013).
42. Gao, X. et al. Soil Hg lability and organo-mineral binding: Constraints from δ13C-SOC and sequestration-redox. *Commun. Ear. Environ.* (under consideration since July) (2025).
43. Yu, G. H. et al. Fungal nanophase particles catalyze iron transformation for oxidative stress removal and iron acquisition. *Curr. Biol.* **30**, 2943–2950 (2020).
44. Gao, X. et al. Tracing the source and transport of hg during pedogenesis in strongly weathered tropical soil using hg isotopes. *Geochim. Cosmochim. Acta*. **361**, 101–112 (2023).
45. Roth, V. N. et al. Persistence of dissolved organic matter explained by molecular changes during its passage through soil. *Nat. Geosci.* **12**, 755–761 (2019).
46. Swift, R. S. Chapter 35. Organic matter characterization. *Methods Soil. Anal. Part. 3 Chem. Methods* 1011–1069 (1996).
47. Lamar, R. T., Olk, D. C., Mayhew, L. & Bloom, P. R. A new standardized method for quantification of humic and fulvic acids in humic ores and commercial products. *J. AOAC Int.* **97**, 721–730 (2014).
48. Tadini, A. M. et al. Soil organic matter in podzol horizons of the Amazon region: Humification, recalcitrance, and dating. *Sci. Total Environ.* **613**, 160–167 (2018).
49. Prentice, A. J. & Webb, E. A. A comparison of extraction techniques on the stable carbon-isotope composition of soil humic substances. *Geoderma* **155**, 1–9 (2010).
50. Ikeya, K. & Watanabe, A. Direct expression of an index for the degree of humification of humic acids using organic carbon concentration. *Soil. Sci. plant. Nutr.* **49**, 47–53 (2003).
51. Kuwatsuka, S., Watanabe, A., Itoh, K. & Arai, S. Comparison of two methods of Preparation of humic and fulvic acids, IHSS method and NAGOYA method. *Soil. Sci. Plant. Nutr.* **38**, 23–30 (1992).
52. Guigue, J. et al. Water-extractable organic matter linked to soil physico-chemistry and microbiology at the regional scale. *Soil. Biol. Biochem.* **84**, 158–167 (2015).
53. Gao, L., Zhou, Z., Reyes, A. V. & Guo, L. Yields and characterization of dissolved organic matter from different aged soils in Northern Alaska. *J. Geophys. Res. Biogeosciences*. **123**, 2035–2052 (2018).
54. Mohinuzzaman, M. et al. Insights into solubility of soil humic substances and their fluorescence characterisation in three characteristic soils. *Sci Total Environ* **720**, (2020).

55. Rosa, A. H. et al. Influence of alkaline extraction on the characteristics of humic substances in Brazilian soils. *Thermochim Acta*. **433**, 77–82 (2005).
56. Wen, H. et al. Asymmetric responses of soil organic carbon stability to shifting dominance of pH-mediated metal-bound organic carbon. *Commun. Earth Environ.* **6**, 574 (2025).
57. Provenzano, M. R., Caricasole, P., Brunetti, G. & Senesi, N. Dissolved organic matter extracted with water and a saline solution from different soil profiles. *Soil. Sci.* **175**, 255–262 (2010).
58. Nkhili, E., Guyot, G., Vassal, N. & Richard, C. Extractability of water-soluble soil organic matter as monitored by spectroscopic and chromatographic analyses. *Environ. Sci. Pollut Res.* **19**, 2400–2407 (2012).
59. Chantigny, M. H., Harrison-Kirk, T., Curtin, D. & Beare, M. Temperature and duration of extraction affect the biochemical composition of soil water-extractable organic matter. *Soil. Biol. Biochem.* **75**, 161–166 (2014).
60. Curtin, D., Beare, M. H., Qiu, W. & Chantigny, M. H. Temperature dependence of organic matter solubility: influence of biodegradation during Soil-Water extraction. *Soil. Sci. Soc. Am. J.* **79**, 858–863 (2015).
61. Fest, E. P. M. J., Temminghoff, E. J. M., Comans, R. N. J. & Van Riemsdijk, W. H. Partitioning of organic matter and heavy metals in a sandy soil: effects of extracting solution, solid to liquid ratio and pH. *Geoderma* **146**, 66–74 (2008).
62. Shi, W. et al. Nature differences of humic acids fractions induced by extracted sequence as explanatory factors for binding characteristics of heavy metals. *Ecotoxicol. Environ. Saf.* **154**, 59–68 (2018).
63. Kleber, M. & Lehmann, J. Humic substances extracted by alkali are invalid proxies for the dynamics and functions of organic matter in terrestrial and aquatic ecosystems. *J. Environ. Qual.* **48**, 207–216 (2019).
64. Whalen, E. D., Grandy, A. S., Geyer, K. M., Morrison, E. W. & Frey, S. D. Microbial trait multifunctionality drives soil organic matter formation potential. *Nat. Commun.* **15**, 10209 (2024).
65. Possinger, A. R. et al. Organo-organic and organo-mineral interfaces in soil at the nanometer scale. *Nat. Commun.* **11**, 6103 (2020).
66. Davidson, E. A., Samanta, S., Caramori, S. S. & Savage, K. The D Ual A Rrhenius and M ichaelis-M enten kinetics model for decomposition of soil organic matter at hourly to seasonal time scales. *Glob Chang. Biol.* **18**, 371–384 (2012).
67. Hilton, R. G. & West, A. J. Mountains, erosion and the carbon cycle. *Nat. Rev. Earth Environ.* **1**, 284–299 (2020).
68. Pietikäinen, J., Pettersson, M. & Bååth, E. Comparison of temperature effects on soil respiration and bacterial and fungal growth rates. *FEMS Microbiol. Ecol.* **52**, 49–58 (2005).
69. Schlesinger, W. H. An evaluation of abiotic carbon sinks in deserts. *Glob Chang. Biol.* **23**, 25–27 (2017).
70. Leake, J. et al. Networks of power and influence: the role of mycorrhizal mycelium in controlling plant communities and agroecosystem functioning. *Can. J. Bot.* **82**, 1016–1045 (2004).
71. Meeks, J. C. & Elhai, J. Regulation of cellular differentiation in filamentous cyanobacteria in free-living and plant-associated symbiotic growth States. *Microbiol. Mol. Biol. Rev.* **66**, 94–121 (2002).
72. Franche, C., Lindström, K. & Elmerich, C. Nitrogen-fixing bacteria associated with leguminous and non-leguminous plants. (2009).
73. Lange, O. L., Belnap, J. & Reichenberger, H. Photosynthesis of the cyanobacterial soil-crust lichen Collema tenax from arid lands in Southern Utah, USA: role of water content on light and temperature responses of CO2 exchange. *Funct. Ecol.* **12**, 195–202 (1998).
74. Protoschill-Krebs, G. & Kesselmeier, J. Enzymatic pathways for the consumption of carbonyl sulphide (COS) by higher plants. *Bot. Acta*. **105**, 206–212 (1992).
75. Asaf, D. et al. Ecosystem photosynthesis inferred from measurements of carbonyl sulphide flux. *Nat. Geosci.* **6**, 186–190 (2013).
76. Whelan, M. E. et al. Soil carbonyl sulfide (OCS) fluxes in terrestrial ecosystems: an empirical model. *J. Geophys. Res. Biogeosciences*. **127**, e2022JG006858 (2022).
77. Kitz, F. et al. Soil COS exchange: A comparison of three European ecosystems. *Global Biogeochem. Cycles*. **34**, e2019GB006202 (2020).
78. Meredith, L. K. et al. Coupled biological and abiotic mechanisms driving carbonyl sulfide production in soils. *Soil. Syst.* **2**, 37 (2018).
79. Whelan, M. E. et al. Carbonyl sulfide exchange in soils for better estimates of ecosystem carbon uptake. *Atmos. Chem. Phys.* **16**, 3711–3726 (2016).
80. Huang, W. & Hall, S. J. Elevated moisture stimulates carbon loss from mineral soils by releasing protected organic matter. *Nat Commun* **8**, (2017).
81. Huang, W. & Hall, S. J. Elevated moisture stimulates carbon loss from mineral soils by releasing protected organic matter. *Nat. Commun.* **8**, 1774 (2017).
82. Whelan, M. E., Min, D. H. & Rhew, R. C. Salt marsh vegetation as a carbonyl sulfide (COS) source to the atmosphere. *Atmos. Environ.* **73**, 131–137 (2013).
83. Sauze, J. et al. The interaction of soil phototrophs and fungi with pH and their impact on soil CO2, CO18O and OCS exchange. *Soil. Biol. Biochem*. **115**, 371–382 (2017).
84. Hansel, C. M., Zeiner, C. A., Santelli, C. M. & Webb, S. M. Mn (II) oxidation by an ascomycete fungus is linked to superoxide production during asexual reproduction. *Proc. Natl. Acad. Sci.* 109, 12621–12625 (2012).
85. Kneip, C., Lockhart, P., Vob, C. & Maier, U. G. Nitrogen fixation in eukaryotes-new models for symbiosis. *BMC Evol. Biol.* **7**, 1–12 (2007).
86. Rockmann, T., Kaiser, J. & Brenninkmeijer, C. A. M. The isotopic fingerprint of the pre-industrial and the anthropogenic N 2 O source. *Atmos. Chem. Phys.* **3**, 315–323 (2003).
87. Buchwald, C., Grabb, K., Hansel, C. M. & Wankel, S. D. Constraining the role of iron in environmental nitrogen transformations: dual stable isotope systematics of abiotic NO2 – reduction by Fe (II) and its production of N2O. *Geochim. Cosmochim. Acta*. **186**, 1–12 (2016).
88. Stern, N. et al. Dual role of humic substances as electron donor and shuttle for dissimilatory iron reduction. *Environ. Sci. Technol.* **52**, 5691–5699 (2018).
89. Zhao, C. et al. The dual roles of dissimilatory iron reduction in the carbon cycle: the iron mesh effect can increase inorganic carbon sequestration. *Glob Chang. Biol.* **30**, e17239 (2024).
90. Boyd, R. J. A quantum mechanical explanation for hund's multiplicity rule. *Nature* **310**, 480–481 (1984).
91. Wu, F. C., Mills, R. B., Evans, R. D. & Dillon, P. J. Kinetics of Metal-Fulvic acid complexation using a Stopped-Flow technique and Three-Dimensional excitation emission fluorescence spectrophotometer. *Anal. Chem.* **76**, 110–113 (2004).
92. Stetten, L. et al. Redox fluctuations and organic complexation govern uranium redistribution from U (IV)-phosphate minerals in a mining-polluted wetland soil, Brittany, France. *Environ. Sci. Technol.* **52**, 13099–13109 (2018).
93. Fortier, S. & Hayton, T. W. Oxo ligand functionalization in the uranyl ion (UO22+). *Coord. Chem. Rev.* **254**, 197–214 (2010).
94. Alexandratos, V. G., Behrends, T. & Van Cappellen, P. Sulfidization of lepidocrocite and its effect on uranium phase distribution and reduction. *Geochim. Cosmochim. Acta*. **142**, 570–586 (2014).
95. Li, Z., Cornelis, J. T., Vander Linden, C., Van Ranst, E. & Delvaux, B. Neoformed aluminosilicate and phytogenic silica are competitive sinks in the silicon soil-plant cycle. *Geoderma* **368**, 114308 (2020).
96. Cuadros, J. Clay minerals interaction with microorganisms: a review. *Clay Min.* **52**, 235–261 (2017).
97. Chen, C. & Thompson, A. Ferrous iron oxidation under varying pO2 levels: the effect of Fe (III)/Al (III) oxide minerals and organic matter. *Environ. Sci. Technol.* **52**, 597–606 (2018).

98. Yu, G. H. et al. Binding of organic ligands with Al(III) in dissolved organic matter from soil: implications for soil organic carbon storage. *Environ. Sci. Technol.* **46**, 6102–6109 (2012).
99. Deguillaume, L. et al. Transition metals in atmospheric liquid phases: Sources, reactivity, and sensitive parameters. *Chem. Rev.* **105**, 3388–3431 (2005).
100. Keiluweit, M. et al. Long-term litter decomposition controlled by manganese redox cycling. *Proc. Natl. Acad. Sci.* **112**, E5253–E5260 (2015).
101. Moffett, J. W. & Zika, R. G. Measurement of copper (I) in surface waters of the subtropical Atlantic and Gulf of Mexico. *Geochim. Cosmochim. Acta*. **52**, 1849–1857 (1988).
102. Diccianni, J., Lin, Q. & Diao, T. Mechanisms of nickel-catalyzed coupling reactions and applications in alkene functionalization. *Acc. Chem. Res.* **53**, 906–919 (2020).
103. Debure, M. et al. Influence of soil redox state on mercury sorption and reduction capacity. *Sci. Total Environ.* **707**, 136069 (2020).
104. Wang, D. et al. Pyrogenic carbon initiated the generation of hydroxyl radicals from the oxidation of sulfide. *Environ. Sci. Technol.* **55**, 6001–6011 (2021).
105. Zheng, W. et al. Mercury stable isotope fractionation during abiotic dark oxidation in the presence of thiols and natural organic matter. *Environ. Sci. Technol.* **53**, 1853–1862 (2019).
106. Buschmann, J. et al. Arsenite and arsenate binding to dissolved humic acids: influence of pH, type of humic acid, and aluminum. *Environ. Sci. Technol.* **40**, 6015–6020 (2006).
107. Kulp, T. R. et al. Arsenic (III) fuels anoxygenic photosynthesis in hot spring biofilms from Mono Lake, California. *Science (80-.).* 321, 967–970 (2008).
108. Mitsunobu, S., Harada, T. & Takahashi, Y. Comparison of antimony behavior with that of arsenic under various soil redox conditions. *Environ. Sci. Technol.* **40**, 7270–7276 (2006).
109. Langmuir, D., Mahoney, J. & Rowson, J. Solubility products of amorphous ferric arsenate and crystalline scorodite (FeAsO4.2H2O) and their application to arsenic behavior in buried mine tailings. *Geochim. Cosmochim. Acta.* **70**, 2942–2956 (2006).
110. Bowell, R. J. Sorption of arsenic by iron oxides and oxyhydroxides in soils. *Appl. Geochem.* **9**, 279–286 (1994).
111. Owings, S. M., Luther, I. I. I., Taillefert, M. & G. W. & Development of a rate law for arsenite oxidation by manganese oxides. *Geochim. Cosmochim. Acta*. **250**, 251–267 (2019).
112. Raven, K. P., Jain, A. & Loeppert, R. H. Arsenite and arsenate adsorption on ferrihydrite: kinetics, equilibrium, and adsorption envelopes. *Environ. Sci. Technol.* **32**, 344–349 (1998).
113. Hopf, J., Langenhorst, F., Pollok, K., Merten, D. & Kothe, E. Influence of microorganisms on biotite dissolution: an experimental approach. *Geochemistry* **69**, 45–56 (2009).
114. Antonangelo, J. A., Ferrari, J., Crusciol, C. A. C. & Alleoni, L. R. F. Lime and calcium-magnesium silicate in the ionic speciation of an oxisol. *Sci. Agric.* **74**, 317–333 (2017).
115. Bigham, J. M., Bhatti, T. M., Vuorinen, A. & Tuovinen, O. H. Dissolution and structural alteration of phlogopite mediated by proton attack and bacterial oxidation of ferrous iron. *Hydrometallurgy* **59**, 301–309 (2001).
116. Shiraki, K. Geochemical behavior of chromium. *Shigen-Chishitsu* **47**, 319–330 (1997).
117. Fuller, A. J., Shaw, S., Peacock, C. L., Trivedi, D. & Burke I. T. EXAFS study of Sr sorption to illite, goethite, chlorite, and mixed sediment under hyperalkaline conditions. *Langmuir* **32**, 2937–2946 (2016).
118. Chen, C. C. & Hayes, K. F. X-ray absorption spectroscopy investigation of aqueous Co (II) and Sr (II) sorption at clay–water interfaces. *Geochim. Cosmochim. Acta*. **63**, 3205–3215 (1999).
119. Bowers, G. M., Ravella, R., Komarneni, S. & Mueller, K. T. NMR study of strontium binding by a micaceous mineral. *J. Phys. Chem. B*. **110**, 7159–7164 (2006).
120. Gransee, A. & Fuhrs, H. Magnesium mobility in soils as a challenge for soil and plant analysis, magnesium fertilization and root uptake under adverse growth conditions. *Plant. Soil.* **368**, 5–21 (2013).
121. Trave, A., Selloni, A., Goursot, A., Tichit, D. & Weber, J. First principles study of the structure and chemistry of Mg-based hydrotalcite-like anionic clays. *J. Phys. Chem. B*. **106**, 12291–12296 (2002).
122. Bufe, A. et al. Co-variation of silicate, carbonate and sulfide weathering drives CO2 release with erosion. *Nat. Geosci.* **14**, 211–216 (2021).
123. Guedron, S., Grangeon, S., Lanson, B. & Grimaldi, M. Mercury speciation in a tropical soil association; consequence of gold mining on hg distribution in French Guiana. *Geoderma* **153**, 331–346 (2009).
124. Barkay, T., Miller, S. M. & Summers, A. O. Bacterial mercury resistance from atoms to ecosystems. *FEMS Microbiol. Rev.* **27**, 355–384 (2003).
125. Misiak, M. et al. Inhibitory effects of climate change on the growth and extracellular enzyme activities of a widespread Antarctic soil fungus. *Glob Chang. Biol.* **27**, 1111–1125 (2021).
126. Kirsten, M. et al. Iron oxides and aluminous clays selectively control soil carbon storage and stability in the humid tropics. *Sci. Rep.* **11**, 5076 (2021).
127. Li, L. et al. New advances in fluorescence excitation-emission matrix spectroscopy for the characterization of dissolved organic matter in drinking water treatment: A review. *Chem. Eng. J.* **381**, 122676 (2020).
128. *Tianjin Statistical Yearbook*. (2019).
129. Kothawala, D. N., Murphy, K. R., Stedmon, C. A., Weyhenmeyer, G. A. & Tranvik, L. J. Inner filter correction of dissolved organic matter fluorescence. *Limnol. Oceanogr. Methods*. **11**, 616–630 (2013).
130. Andersson, C. A. & Bro, R. The N-way toolbox for MATLAB. *Chemom Intell. Lab. Syst.* **52**, 1–4 (2000).
131. Stedmon, C. A., Markager, S. & Bro, R. Tracing dissolved organic matter in aquatic environments using a new approach to fluorescence spectroscopy. *Mar. Chem.* **82**, 239–254 (2003).
132. Mostofa, K. M. G., Jie, Y., Sakugawa, H. & Liu, C. Q. Equal treatment of different EEM data on PARAFAC modeling produces artifact fluorescent components that have misleading biogeochemical consequences. *Environ. Sci. Technol.* **53**, 561–563 (2019).
133. Reis Ely, C. R. et al. Global terrestrial nitrogen fixation and its modification by agriculture. *Nature* **643**, 705–711 (2025).
134. Whalen, E. D. et al. Microbial trait multifunctionality drives soil organic matter formation potential. *Nat. Commun.* **15**, 10209 (2024).
135. Hansel, C. M. et al. Mn(II) oxidation by an ascomycete fungus is linked to superoxide production during asexual reproduction. *PNAS* **109**, 12621–12625 (2012).
136. Wang, D. et al. Pyrogenic Carbon Initiated the Generation of Hydroxyl Radicals from the Oxidation of Sulfide. *Environ. Sci. Technol.* 2021, 55, 6001 – 6011 (2021).
137. Yang, X. et al. New insights into mechanisms of sunlight- and dark-mediated high-temperature can accelerate diurnal production-degradation transformation of lake fluorescent DOM. *Sci. Total Environ.* **760**, 143377. https://doi.org/10.1016/j.scitotenv.2020.143377 (2021).
138. *Tianjin Bureau of Statistics*. (2019).
139. Yuan, J. et al. Denitrification devices in urban boilers change mercury isotope fractionation signatures of coal combustion products. *Environ. Pollut.* **268**, 115753 (2021).

Acknowledgements

This study was supported by the National Natural Science Foundation of China (42293262, 41925002, U1612441

and 42230509) and also by the Key Construction Program of the National "985" Project, Tianjin University, China.

Author contributions

K.M.G.M. and C.Q.L. designed, planned and supervised the study. M.M. performed all experimental analysis, analytical measurements and data analyses. J.Z. helped in the laboratory analysis. R.S. and W.Z. performed Hg analysis. J.Y. performed the EEM-PARAFAC analysis. K.M.G.M., N.S. and M.M. wrote the manuscript, with critical inputs from G.S.N., S.L.S. and all other co-authors. D.V. and J.C. edited and revised the manuscript.

Declarations

Competing interests

The authors declare no competing interests.

Additional information

Supplementary Information The online version contains supplementary material available at https://doi.org/10.1038/s41598-025-20429-4.

Correspondence and requests for materials should be addressed to M.G.K.M. or C.-Q.L.

Reprints and permissions information is available at www.nature.com/reprints.

Publisher's note Springer Nature remains neutral with regard to jurisdictional claims in published maps and institutional affiliations.